



Perovskite Solar Cells

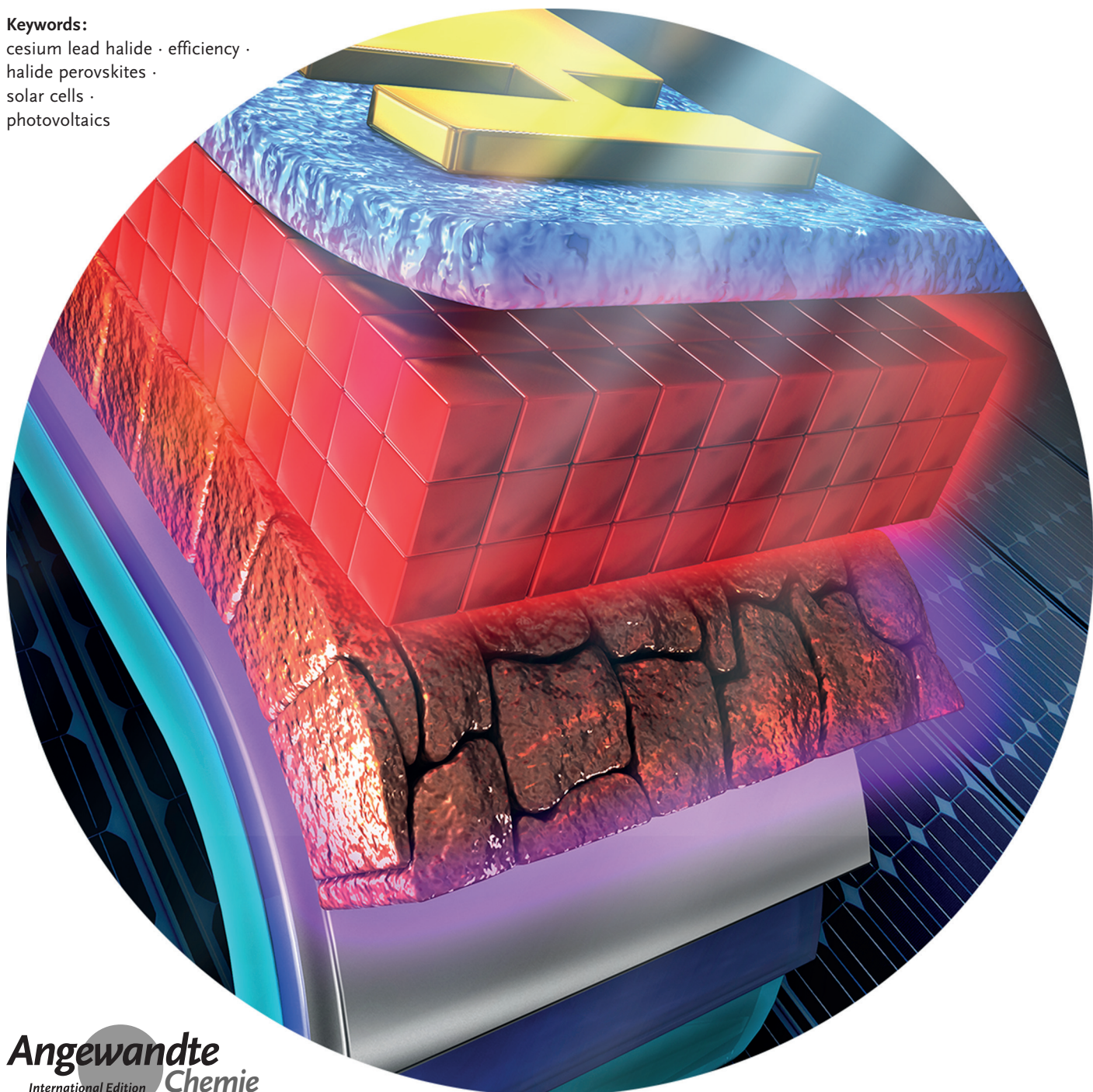
International Edition: DOI: 10.1002/anie.201901081
German Edition: DOI: 10.1002/ange.201901081

All-Inorganic CsPbX₃ Perovskite Solar Cells: Progress and Prospects

Jingru Zhang⁺, Gary Hodes⁺, Zhiwen Jin,* and Shengzhong (Frank) Liu*

Keywords:

cesium lead halide · efficiency ·
halide perovskites ·
solar cells ·
photovoltaics



Recently, lead halide-based perovskites have become one of the hottest topics in photovoltaic research because of their excellent optoelectronic properties. Among them, organic-inorganic hybrid perovskite solar cells (PSCs) have made very rapid progress with their power conversion efficiency (PCE) now at 23.7 %. However, the intrinsically unstable nature of these materials, particularly to moisture and heat, may be a problem for their long-term stability. Replacing the fragile organic group with more robust inorganic Cs^+ cations forms the cesium lead halide system (CsPbX_3 , X is halide) as all-inorganic perovskites which are much more thermally stable and often more stable to other factors. From the first report in 2015 to now, the PCE of CsPbX_3 -based PSCs has abruptly increased from 2.9 % to 17.1 % with much enhanced stability. In this Review, we summarize the field up to now, propose solutions in terms of development bottlenecks, and attempt to boost further research in CsPbX_3 PSCs.

1. Introduction

Environmental pollution caused by fossil fuel combustion together with the decreasing costs of photovoltaic cells has resulted in a major increase in the commercial use of these cells. In fact, in 2017 alone, over 100 GW of solar modules have been installed worldwide, dominated by crystalline silicon modules, the first generation cells.^[1] The main disadvantage of crystalline silicon cells are the high temperature/energy processing costs including the relatively long (typically 1–2 years) energy payback time with secondary disadvantage, depending on application, of relatively poor performance at high temperature and under weak light conditions, as well as being rigid and relatively heavy.^[2] Thin-film solar cells based on amorphous Si, CdTe or Cu(In,Ga)Se₂ form the second generation of commercial cells,^[3] and make up approximately 5 % of the total manufactured modules in 2017. Third generation cells include a range of thin-film cells, including dye-sensitized,^[4] polymer,^[5] quantum dot,^[6] and halide perovskite (HaP) cells.^[7] The HaPs, which are the subject of this Review, are a particularly exciting set of semiconductors combining many excellent properties at the same time, including large carrier diffusion lengths (due mainly to long charge lifetimes), tolerance to defects/low defect densities and large optical absorption coefficients near the band gap.^[8] In fact, since its discovery in 2009, the efficiency of HaP solar cells has increased from 3.8 % to 23.7 %.^[9,10]

In its general formula ABX_3 , the A site is a monovalent cation, the B site Pb (less commonly Sn) and the X site halide anions. The A cation has to be large enough to permit formation of the perovskite phase (see more details in Section 2.1). The most common cations are methylammonium (MA), formamidinium (FA)), and Cs. Cations that are substantially larger or smaller will not allow formation of the desired three-dimensional perovskite phase although they may be used together with the aforementioned cations in small concentrations to fine-tune the structure. Besides

From the Contents

1. Introduction	15597
2. Structure and Performance	15598
3. Fabrication Methods	15602
4. Solar Cells	15603
5. Conclusions and Prospects	15614

allowing formation of the perovskite phase, the size of the A cation also affects details of the structure (also discussed in more detail in Section 2.1). However the A cation does not directly (to some extent, it does indirectly) affect the band gap of the semiconductor.^[11] Unfortunately, all the highest efficiency cells so far use the organic-inorganic hybrid perovskite (although often with a small percentage of inorganic A cation^[12]) in which the organic A component is less stable than the inorganic one, particularly under thermal stress as the organic species are lost at relatively low temperatures.^[13] Since the long-term stability of these cells is the main bottleneck before it moves into commercialization, using materials without organic cations therefore confers an advantage in terms of stability.^[14] From the first reports in 2015 to now, the PCE of CsPbX_3 based PSCs have increased from 5.8 % (CsPbBr_3)^[15] and 2.9 % (CsPbI_3)^[16] to 17.1 % (CsPbI_3)^[17] together with increasing stability. From this progress, CsPbX_3 materials are emerging as a new research

[*] J. Zhang^[+]

Key Laboratory of Applied Surface and Colloid Chemistry, Ministry of Education, Shaanxi Key Laboratory for Advanced Energy Devices, Shaanxi Engineering Lab for Advanced Energy Technology, School of Materials Science & Engineering, Shaanxi Normal University Xi'an, 710119 (P. R. China)

Prof. Z. Jin

School of Physical Science and Technology & Key Laboratory for Magnetism and Magnetic Materials of the Ministry of Education, Lanzhou University
Lanzhou, 730000 (P. R. China)
E-mail: jinzw@lzu.edu.cn

Prof. S. Liu

Dalian National Laboratory for Clean Energy, iChEM, Dalian Institute of Chemical Physics, Chinese Academy of Sciences
Dalian, 116023 (P. R. China)
E-mail: szliu@dicp.ac.cn

Prof. G. Hodes^[+]

Department of Materials and Interfaces, Weizmann Institute of Science
Rehovot, 76100 (Israel)

[†] These authors contributed equally to this work.

 The ORCID identification number(s) for the author(s) of this article can be found under:
<https://doi.org/10.1002/anie.201901081>.

area and will play a significant role in the photovoltaic field in the near future.^[18]

Herein, we Review the development of inorganic HaPs with the general formula CsPbX_3 and their related solar cells. While some of the best HaP cells often contain a small amount of Cs in the A cation mix, which is usually beneficial for the stability (attributed to the enhanced interaction between ions through contraction of cubo-octahedral volume),^[19–21] herein we consider only semiconductors where the A cation is 100% (or nearly 100%) Cs. This Review is divided into four parts: in the first Section, we discuss the CsPbX_3 materials performance in general, focusing on the crystalline structure, electronic structure, photo-physical properties, and compositional stability; in the second Section, the mainstream fabrication routes—solution- and vapor-deposition—of CsPbX_3 films are briefly introduced; the third Section covers the recent progress and strategies to obtain high efficiency and stabilized CsPbX_3 PSCs. Finally, challenges and perspective of the future development of all-inorganic CsPbX_3 PSCs are presented.

2. Structure and Performance

It is well established that the photo-physical properties and the compositional stability of the semiconductors are closely related to the crystal and electronic structures.^[22] To study the CsPbX_3 family in depth, we discuss the CsPbX_3 materials performance, mainly focusing on the crystalline structure, electronic structure, photophysical properties, and compositional stability.



Jingru Zhang received her B.S. degree in Materials Chemistry from Shaanxi Normal University of China in 2015. She is currently a M.S. of Prof. Shengzhong (Frank) Liu and Prof. Zhiwen Jin at Shaanxi Normal University. Most recently her research interest focuses on all-inorganic perovskite solar cells.



Gary Hodes is a Professor Emeritus at the Weizmann Institute of Science, Rehovot, Israel. He received a BSc and PhD, both from Queen's University, Belfast. He has worked in two main and connected fields: solution deposition of semiconductor films, including quantum dots and nanostructured films, and various types of photoelectrochemical and photovoltaic cells. He is currently working on photovoltaic cells based on halide perovskites.

2.1. Crystalline Structure

CsPbX_3 has four types of crystal polymorph (shown in Figure 1a):^[23] the cubic structure (α -, $Pm\bar{3}m$); the tetragonal structure (β -, $P4/mmb$), the orthorhombic structure (γ -, $Pbnm$); and a non-perovskite structure (δ -, $Pnma$). Thus, for example the RT stable phase of CsPbI_3 is the non-perovskite δ - yellow phase that is relatively inactive as a photovoltaic material, while what is known as the black (α -) phase is only stable at RT under special conditions. There are also two other black phases (β and γ) that are considerably less common.^[24] On the other hand the stable form of CsPbBr_3 at RT is the γ , orthorhombic form. In the perovskite structure of CsPbX_3 , the Pb^{2+} and X^- ions form a 3D network of corner-sharing PbX_6 octahedra, and the Cs^+ ions occupy the octahedral voids created by the halogens.^[25] As the temperature decreases from where the “high”-temperature cubic phase is stable, the PbX_6 octahedra in the cubic phase will increasingly tilt and the crystal structure will transform from the cubic to the lower-symmetry tetragonal and then orthorhombic forms.^[26,27]

The structural (phase) stability of ABX_3 (the generic perovskite composition) is determined largely by the volumetric ratio between the BX_6 octahedra and the A cation. The formation of the perovskite structure can be predicted from the Goldschmidt tolerance factor, t , where t is given by Equation (1):^[28,29]

$$t = (r_{\text{A}} + r_{\text{X}}) / (2^{1/2}[r_{\text{B}} + r_{\text{X}}]) \quad (1)$$



Zhiwen Jin is a professor with the School of Physical Science and Technology, Lanzhou University. He received the B.S. degree from Lanzhou University in 2011 and Ph.D. degree from Institute of Chemistry, Chinese Academy of Sciences in 2016. From 2016 to 2018, he was a Post-Doctoral Fellow with Shaanxi Normal University. He joined Lanzhou University in 2018. His research interests include inorganic semiconductor materials, photoelectric devices and photovoltaic cells based on CsPbX_3 perovskites.



Shengzhong (Frank) Liu received his Ph.D. degree from Northwestern University (Evanston, Illinois, USA) in 1992. Upon his post-doctoral research at Argonne National Laboratory (Argonne, Illinois, USA), he joined high-tech companies in US for research including nanoscale materials, thin film solar cells, laser processing, diamond thin films, etc. His invention at BP Solar in semi-transparent photovoltaic module won the R&D 100 award in 2002. In 2011, he was selected into China's top talent recruitment program and now he is a professor at Shaanxi Normal University and Dalian Institute of Chemical Physics, Chinese Academy of Sciences.

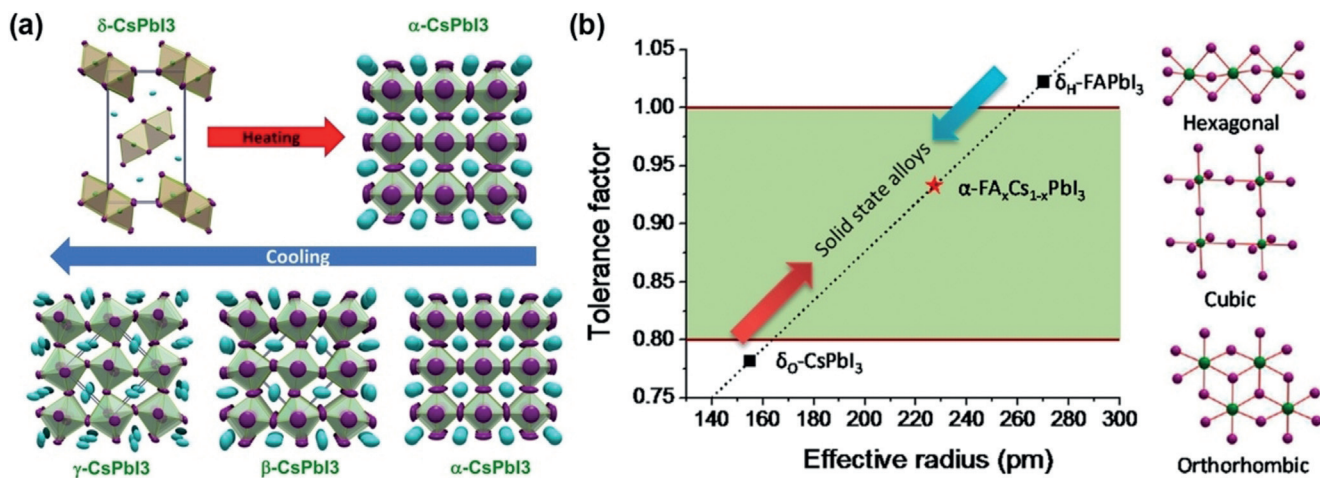


Figure 1. a) Structural phase transitions. Reproduced with permission.^[23] Copyright 2015, American Chemical Society Publications. b) Correlations between tolerance factor and crystal structure of APbI₃ perovskite materials. Reproduced with permission.^[29] Copyright 2016, American Chemical Society Publications.

where r_A , r_X , and r_B are ionic radii for A, X, and B sites, respectively. The t is therefore a determinant of structural stability.^[30] A cubic perovskite structure can, as a general rule, be obtained if t is between 0.9 and 1 (shown in Figure 1b). However, a perovskite can form when $0.8 \leq t \leq 1$, although the perovskite structure will be distorted as the tolerance factor decreases below around 0.9 because of the BX₆ octahedra tilting. The A-site cation is too large to form a perovskite configuration when $t > 1$, whereas when $t < \approx 0.8$, the A-site cation is too small to form the perovskite.^[31] For CsPbI₃, the undesirable phase transition is because the size of the Cs⁺ cation is too small (Cs⁺, with an ionic radius of 1.81 Å, is considerably smaller than the organic ones MA⁺ (2.70 Å) or FA⁺ (2.79 Å)).

For CsPbI₃, t is 0.81–0.84 (depending on which values of ionic radii are used) which limits its black α-phase stability. Changing the halide to smaller Br or Cl increases the value of t by a small amount (by ca. 1 % for the Br and a further ca. 1 % for the Cl; however, this is apparently enough to stabilize the room-temperature perovskite forms to orthorhombic for CsPbBr₃ and the unusual monoclinic for CsPbCl₃. CsPbCl₃ exists in a number of different phases just above room temperature (for a tabulation of the phase relations with temperature of the various CsPbX₃ (and CsSnX₃), see Table 1 in Ref. [32].

2.2. Electronic Structure

Theoretical calculations of electronic structure are very useful to estimate the basic electrical and optical properties of semiconductors. Density functional theory (DFT) studies have been widely used to theoretically predict the electronic structure of CsPbX₃.^[33,34] It has been found that the electronic structures of CsPbX₃ with different halide compositions have showed qualitatively common features. In theory, for CsPbX₃ in general, the valence band maximum (VBM) is mainly

composed of antibonding hybridized Pb 6s and X np orbitals with dominant contributions from X np, while the conduction band minimum (CBM) is determined by antibonding mixing of Pb 6p and X np orbitals, with the major contribution from Pb 6p (shown in Figure 2a).^[35]

Based on DFT, taking into account relativistic corrections and spin-orbit interactions, the band structures are almost independent of the halide composition, except for the difference in the band gap (E_g) values, and all the CsPbX₃ perovskites show a direct E_g, indicating their potential application in optoelectronics.^[36] The Cs, as for the organic A cations, has little direct effect on the electronic structure near the band edge, although it can affect it indirectly through tilting of the PbI₆ octahedral. Therefore, the excitation and recombination of electrons and excitons are confined within the PbX₆ octahedra (Figure 2b).^[37,38] For CsPbCl₃ and CsPbBr₃, their geometric structures change little between different phases, while for the CsPbI₃ the larger radius of iodine leads to more significant changes in geometric structures and hence electronic structures, particularly in band gaps.^[39,40]

Experiments also found the dielectric constant (ϵ) for CsPbX₃ is related to the relative motion within the PbI₆ octahedra. The values of binding energy (R*) and effective mass (μ) are increased with increasing band gap energy (shown in Figure 3a), similarly to hybrid HaPs.^[41,42] Small and comparable effective masses of the electrons and holes can be predicted from the electronic band dispersion around the band edges, which contribute to the carrier mobilities.^[43] However these mobilities, in the Pb-based HaPs in general, are considerably smaller than expected from the values of effective mass, and it has been suggested that this is due to phonon scattering by the relatively soft HaP lattice.^[44] As the crystal cubic phase is transformed to the low-symmetry orthorhombic phase, the metal-halide-metal bond angle decreases. Along with the increase in the E_g, this decrease in bond angle increases both the effective carrier masses and

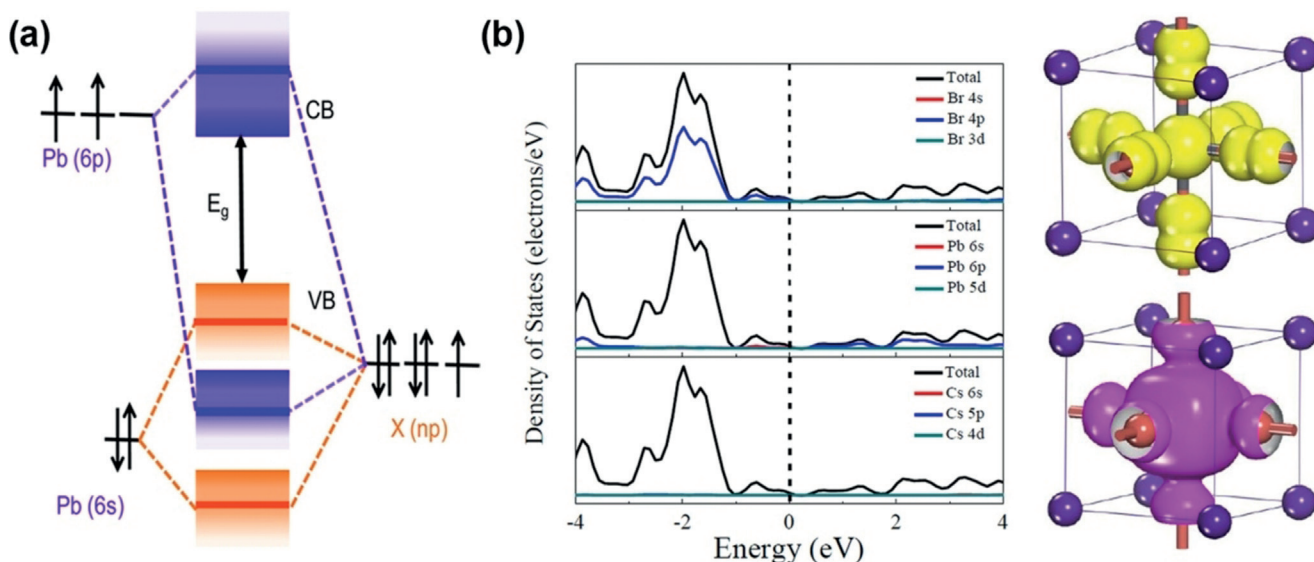


Figure 2. a) Schematic representation of bonding/antibonding orbitals of APbX_3 showing the formation of the VB and CB. Reproduced with permission.^[35] Copyright 2016, American Chemical Society Publications. b) Density of states of cubic CsPbBr_3 with corresponding contributions of elements to the energy bands, and electronic profiles of the VBM and CBM. Reproduced with permission.^[37] Copyright 2016, Wiley-VCH Publications.

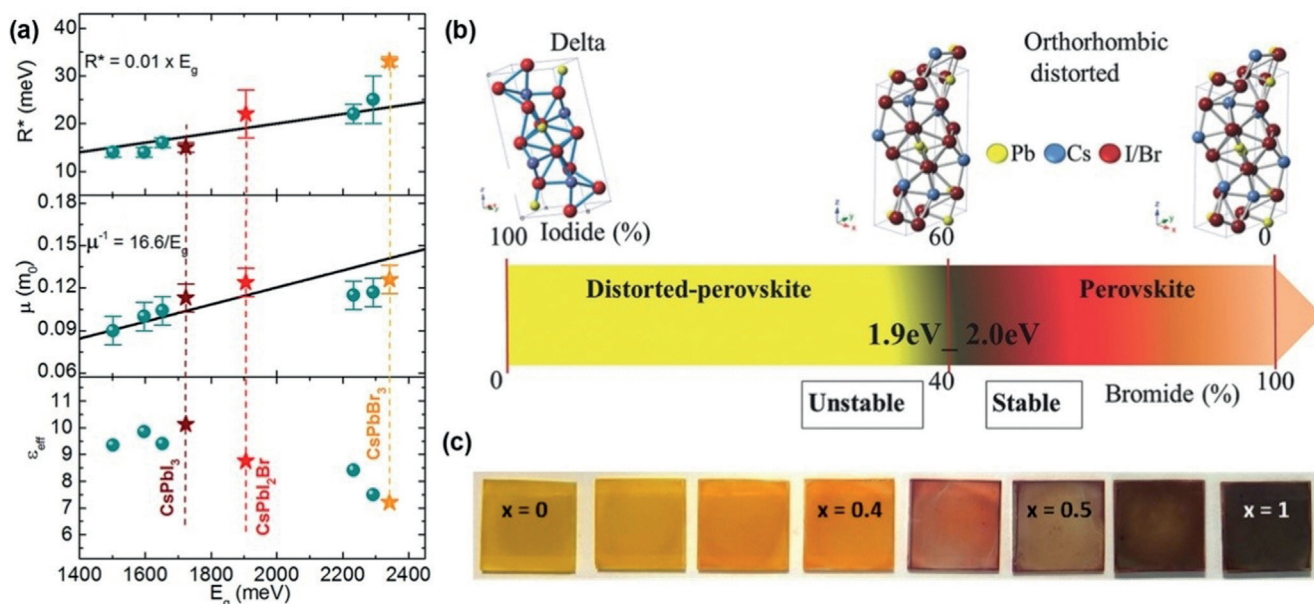


Figure 3. a) Binding energy (R^*), effective mass (μ), and dielectric constant (ϵ) of CsPbX_3 as a function of the band gap (E_g). Brown, red, and yellow stars indicate the results for CsPbI_3 , CsPbI_2Br , and CsPbBr_3 , respectively. Reproduced with permission.^[41] Copyright 2017, American Chemical Society Publications. b) The CsPbX_3 crystal structure as a function of I/Br ratio. Reproduced with permission.^[65] Copyright 2018, Wiley-VCH Publications. c) Photographs for $\text{CsPb}(\text{Br}_{1-x}\text{I}_x)_3$ films. Reproduced with permission.^[155] Copyright 2016, Wiley-VCH Publications.

the number of deep transition defect levels.^[45] Therefore, these results suggest that to make high-performance CsPbX_3 , it is necessary to engineer the structure of CsPbX_3 with a larger metal-halide-metal bond angle, that is, a smaller octahedral tilt.^[46,47]

2.3. Photophysical Properties

The most important parameters for a semiconductor to be used in solar cells are a) the band gap (the optimal value of which will depend on the type of cell: single junction, multijunction or spectrally split); b) the light absorption coefficient; and c) the charge diffusion lengths. The E_g , in

common with some other semiconductor groups, for example, the III-V semiconductors, can be tuned over the entire visible and near IR spectrum. Except to note that, up to now, perovskites with high E_g (mainly the pure bromides or Br-rich compounds) have a greater voltage loss than the iodides (voltage loss will be discussed in Section 4.4.4^[48]), there is nothing special to perovskites in this respect compared to other semiconductors, and we will not consider it further in this Section.

The absorption coefficients, α , are high for the Pb HaPs and the absorption onsets are very sharp (both these are considerably less for the Sn-based HaPs). This means that only a very thin film—typically several hundred nm—is needed to absorb essentially all the super-band gap light. The main importance of this is that it defines the minimum diffusion length, L_d , required to collect all the carriers (ideally several times the film thickness). Therefore the ability to use very thin films translates into the need for lower L_d . It is also worth noting that the Urbach parameter, E_u , which is a measure of sub-band gap tail absorption in the semiconductor, and can be linked to static disorder in the semiconductor, is unusually low (at least for the iodide HaPs). This situation implies low charge trapping, something that has been verified for these materials, particularly in single crystals. The values of L_d of both electrons and holes are particularly high in the HaPs in general. L_d is defined by two parameters—charge mobility and charge lifetime. Charge mobilities in the HaPs are high (if compared to organic semiconductors) or rather low (if compared to other photovoltaic semiconductors). We already noted that charge mobilities are lower than expected based on the effective masses of the HaPs. The high values of L_d in HaPs are mainly due to the long lifetimes.

There is still only limited data on diffusion lengths and their associated parameters (mobilities and charge lifetimes) in CsPbX_3 . It seems that mobility values for Cs lead HaPs are similar to those of the corresponding hybrid ones. Values of approximately $25 \text{ cm}^2 \text{ V}^{-1} \text{ s}^{-1}$ have been reported by several groups for CsPbI_3 ^[49,50] with somewhat smaller (ca. $10 \text{ cm}^2 \text{ V}^{-1} \text{ s}^{-1}$ for CsPbI_2Br)^[51] and larger ($38 \text{ cm}^2 \text{ V}^{-1} \text{ s}^{-1}$ for CsPbBr_3)^[52] values also reported. These values are comparable to typical values for the hybrid Cs HaPs. Charge lifetimes were, not surprisingly, more variable. Hutter et al. compared evaporated and spin-coated CsPbI_3 and reported approximately $10 \mu\text{s}$ for the evaporated films compared to about 200 ns for the spin-coated ones.^[49] Lifetimes of over 20 ns were also reported for the same HaP deposited by solution processing.^[50] For CsPbBr_3 , lifetimes of $2\text{--}7 \mu\text{s}$ for macroscopic single crystals were reported. For solution-processed CsPbI_2Br , a value of around 14 ns was reported.^[53] Regarding diffusion lengths, for solution-processed CsPbI_3 , L_d was estimated to be about $1 \mu\text{m}$,^[50] while for single-crystal CsPbBr_3 , separate values of L_d for electrons and holes were found to be about $10 \mu\text{m}$ and $12 \mu\text{m}$, respectively.^[54] For CsPbBr_3 film, L_d for electrons was 80 nm .^[55] Note in comparing these values that single HaP crystals generally give much higher values of charge lifetime and thus L_d than polycrystalline films do,^[56] as well as lower trap densities: thus it is likely that the long charge lifetimes are, at least to some

extent, connected to the low defect concentration. As with the hybrid HaPs, CsPbX_3 is also a defect-tolerant semiconductor that can maintain its electronic quality despite the presence of defects.^[57] Such defect tolerance has been attributed to the lack of bonding–antibonding interaction between the conduction and valence bands.^[58]

In spite of the above similarities between the Cs and organic cation HaPs, implying that the role of the PbI_6 framework dominates over that of the nature of the A cation, as also pointed out in Refs. [49,59], there remain some differences which relate mainly to doping. It has been reported that self-doping occurs in CsPbI_3 in contrast to the case for MAPbI_3 .^[45] Indeed, it was shown that, for the bromide perovskites, the carrier density of CsPbBr_3 was 3–4 orders of magnitude higher than that for MAPbBr_3 (but not if the MAPbBr_3 was prepared with the addition of Cl ions) as well as compared to mixed A-cation HaP (containing a small percentage of Cs).^[55]

2.4. Compositional and Phase Stability

Long-term stability of the HaPs and their photovoltaic cells is probably the most critical aspect for commercial use. Although the most important stability metric is the power conversion efficiency, there are many different types of stability. Replacing fragile organic moieties with robust inorganic Cs^+ cations can be considered a promising approach to design of more stable materials that can potentially achieve pragmatic operational benchmarks.

One rather obvious stability metric is to heat. Since the organic A^+ cations are rather volatile, while Cs^+ is very much less so, it is not surprising that CsPbX_3 is much more thermally stable than the equivalent hybrid compounds. Thus it was noted that CsPbBr_3 was annealed at 250°C in air for optimum cells^[15] and it was shown that not only is CsPbBr_3 thermally stable up to approximately 550°C but that, when it does start to decompose, it is due to loss of PbBr_2 and not CsBr .^[60]

Mariotti et al. carried out experiments to monitor the effect of different environmental parameters on the stability of CsPbI_2Br .^[61] They found that, of humidity, oxygen, UV light (365 nm), indoor light and UV + O_3 , the only parameter that clearly degraded the HaP was water vapor.^[62] Even then, the change was not decomposition but change in phase, which was reversible on heating. All the other parameters had either no effect (after one month) or, in the case of UV, a slow degradation effect. Another study found that, while MAPbI_3 lost MAI upon exposure to white light (70 mW cm^{-2} at 45°C) over hundreds of hours, CsPbI_3 was unaffected by the same treatment.^[63]

Electron beam irradiation of hybrid HaPs is known to readily damage the HaP and while this may not be a problem for commercial cells, it certainly is a problem when e-beam characterization is carried out, such as SEM, EDS, and cathodoluminescence. The Cs-based HaPs are much more robust during these measurements.^[60,64] This is not surprising since the heat generated in the sample by the e-beam can evaporate the volatile organic constituents but much less readily the inorganic part.

There are two aspects of phase stability that are important. One relates to the fact that the black phase (most commonly the α phase) of CsPbI_3 is thermodynamically unstable under ambient conditions. Adding Br increases the Goldschmidt factor resulting in increased phase stability. Thus mixed $\text{CsPb}(\text{I},\text{Br})_3$ has been extensively studied for this reason (as well as allowing tailoring of the band gap to higher values, Figures 3b,c). Sanchez et al. have reported that at least 40% Br is needed to maintain stability of the $\text{CsPb}(\text{I},\text{Br})$.^[65] The second aspect of phase stability is the phase separation in hybrid HaPs that occurs in $\text{MAPb}(\text{I},\text{Br})$ due to light-enhanced ion migration when Br is over around 15%.^[66] This has been shown to be suppressed in $\text{CsPb}(\text{I},\text{Br})$ up to about 40% Br.^[67] Thus it could be questioned if both “black” (or brown as it can appear) phase stability and stability against segregation can be both obtained for $\text{CsPb}(\text{I},\text{Br})$. Yin et al. found from theoretical calculations that CsPbI_2Br has a particularly stable alloy phase as a result of strong Coulomb interactions in the ionic perovskite lattice.^[68] On an optimistic note, Zhou et al. have demonstrated 1500 hours operational stability (maximum power) of a cell based on CsPbI_2Br .^[67] Apart from the question as to whether both phase stability and stability against segregation can be obtained, this encouraging result demonstrates that cells based on Cs can be stable at least over the medium term.

A final note for this Section concerns the important issue of self-healing, believed to occur in the Cs-based HaPs.^[69–71] One of the advantages of the Cs-based HaPs compared to the hybrid ones is that CsX , being much less volatile than organic cation halides, is much less likely to be lost from the surface of the HaP (or possibly from interfaces with other phases). Therefore even if CsPbX_3 is decomposed by moisture, the CsX will remain to maybe reform the HaP by self-healing. While this type of surface change is likely to be the most relevant one for PV cells, it was found, unexpectedly, that for APbBr_3 , where only intrinsic self-healing (i.e. without environmental effects) was considered by absorbing light well into the bulk of single crystals and far from any surface using 2-photon absorption, while both hybrid and Cs HaPs underwent self-healing after damage from an intense laser beam, the Cs HaP took much longer to heal than the hybrid ones did.^[70]

3. Fabrication Methods

The preparation of CsPbX_3 thin films with pinhole/crack-free surfaces is normally required to prevent electrical shorting through the pinholes/cracks and ensure the high performance of optoelectronic devices using these films.^[72] The most common deposition technique is by solution processing,^[73] but physical vapor deposition (evaporation) is also often used.^[72] In both methods, either a one step or two step deposition have been developed.

3.1. All Solution Method

The advantages of solution methods in general are simple (at least in principle) operation and convenient preparation

with generally low energy costs (particularly for the HaPs which mostly require only low-temperature annealing). The disadvantages are that there are many parameters involved, not all of which are even realized or obvious at first (consider air/gas flow patterns near the substrate or use of antisolvents) which can make the process difficult to reproduce from run to run, as well as the difficulty in preparing large-area, high-efficiency devices. Also solution methods often, though not necessarily, introduce a relatively high concentration of defects.^[74] This is probably less problematic for the defect-tolerant HaPs.

The most commonly used solution-processed method is spin-coating and can be divided into one-step^[75,76] and multi-step^[77,78] techniques.

In one-step methods, the CsPbX_3 precursors are dissolved in the precursor solvent or mixture of solvents at a fixed (often stoichiometric) ratio, and then spin-coated. Common solvents are dimethyl formamide (DMF), dimethyl sulfoxide (DMSO), or a mixture of the two.^[79] A common variation is to introduce a variety of anti-solvents, such as chlorobenzene (CB), benzene, xylene, toluene, isopropylalcohol (IPA), ethyl acetate (EA), and chloroform during the spin-coating.^[80] These anti-solvents increase the rate of HaP or HaP precursor nucleation resulting in improved morphology/coverage of the substrate. The resulting films are then annealed (for hybrid HaPs, at temperatures usually not far from 100°C, but for HaPs without organic A cations, as for CsPbX_3 , higher temperatures are often beneficial). Simple one-step fabrication methods seem to be difficult to control, particularly in terms of reproducibility. For Cs-based HaP films, one of the major constraints for the one-step method is the solubility limit of Cs salts and in particular CsBr (ca. 0.25 M in DMSO, ca. 0.5 M together with PbBr_2).^[81] Early reports have stated that a lack of solubility hindered the fabrication of a sufficiently thick and pinhole-free films.^[82]

In the two-step sequential method, PbX_2 is first deposited usually by spin-coating followed by chemical reaction with CsX (usually in solution) to give the HaP (Figure 2a). Since PbX_2 is generally more soluble in the common solvents than CsX , and particularly so for the bromides, this can solve the problem of relatively low solubility of CsBr . The key parameters for two-step sequential deposition and perovskite conversion by dipping are immersion time, temperature of the conversion solution, and precursor concentration. Two-step methods often give better film morphology than the one-step method although it could be argued that, as there are more parameters that have to be controlled, the method might be expected to be less reproducible.

As mentioned above, one of the major constraints of CsPbX_3 is the solubility limit of Cs and Br precursors, which hindered the fabrication of a sufficiently thick and pinhole-free perovskite film. Hence, solvent optimization is usually conducted: Snaith et al. studied the effects of solvent choice on the electronic, structural, and morphological properties of CsPbI_3 thin films. Their findings reveal the critical impact solvents have upon compositional stoichiometry and thin-film morphology.^[83] Meng et al. reported a method to improve the quality of $\text{CsPb}(\text{I},\text{Br}_{1-x})_3$ films via two-step multiple spin coating. By introduced DMSO into CsBr /methanol precursor,

they obtained the compact and pinhole-free perovskite films. They found introduction of DMSO can improve the solubility of CsBr, which further affect the morphologies, optical properties, and photovoltaic performance of $\text{CsPb}(\text{I},\text{Br}_{1-\alpha})_3$ films.^[84]

Quantum dots (QDs) of CsPbX_3 have been used for photovoltaic cells in several cases. Sols or dispersions of CsPbX_3 QDs were applied as “inks” to fabricate HaP films at room temperature by spin-casting QD sols onto the substrate.^[85,86] This method provides a new pathway for single-step, large-scale fabrication of CsPbX_3 cells. Since the liquid phase does not dissolve the HaP, multiple deposits can be made, allowing any desired film thickness to be formed.^[87] In common with QD photovoltaic cells using other materials, long chain-capping agents, often used in making the QD sol (to prevent aggregation of the QDs) will result in a high electrical resistance and therefore poor charge carrier properties. However, as with other materials, these long chain ligands can be exchanged with shorter (or no) capping agents, leading to much better charge transport.^[88]

3.2. All Vacuum Deposited

Vacuum thermal evaporation is a mature technique used in the coating industry that can easily deposit multiple layers of thin films over large areas, and the deposited films have good uniformity and flatness.^[89] The film thickness can be precisely controlled and the resulting samples show reproducible quality. It has been reported that the charge-carrier lifetimes of vapor-deposited CsPbI_3 films lasts several μs , much longer than those fabricated by spin-coated films. This difference was attributed to a significantly higher defect density in the spin-coated films, acting as charge carrier traps. However, vacuum deposited method needs to accurately control the stoichiometric ratios of the precursors in halides, and usually hard to control the crystal structure.

4. Solar Cells

The performance of PSCs needs to significantly improve in two major aspects: The PCE for large-area cells and their stability. CsPbI_3 , first identified as a photoconductive material in 1958,^[90] has a E_g of 1.73 eV which is very suitable for photovoltaic applications and in particular as a top cell for a tandem on Si. In 2015, Eperon et al. investigated CsPbI_3 PSCs for the first time with a measured stabilized PCE up to 1.7% for a planar heterojunction architecture.^[16] The highest reported stabilized PCE for any CsPbX_3 is 16.3% (for CsPbI_3).^[17] However, CsPbI_3 is thermodynamically unstable in the black phase and tends to go back to the room-temperature-stable yellow phase, even with encapsulation, while the corresponding bromide and chloride are stable in the perovskite phase as already discussed in Section 2.1. Therefore addition of Br to CsPbI_3 can help to stabilize the HaP but at the cost of increasing E_g .

In this Section, we discuss first CsPbI_3 cells where much of the emphasis is on stabilizing the black phase (usually the α -

phase), but also on increasing efficiency. Next we discuss CsPbBr_3 cells, followed by mixed $\text{CsPb}(\text{I},\text{Br})_3$ cells. We note that when giving power conversion efficiencies (PCEs), we prefer to use stabilized PCEs (sPCE) if available. This refers to PCE measured after typically some tens or hundreds of seconds of cell operation when the PCE remains stable over (short) times. Because of the large current–voltage scan-direction hysteresis common in these cells, if sPCE is not given we give a mean between reverse scan and forward scan PCE (rfPCE) where available. If also this is not available, we note the direction of scan or that no direction was given.

4.1. CsPbI_3 Cells

Choi et al. reported the first CsPbI_3 PSC with a PCE of 0.09% (most of that paper was dedicated to mixed $(\text{MA},\text{Cs})\text{PbI}_3$).^[91] Eperon et al. fabricated a CsPbI_3 PSC using an HI additive which gave grain refinement with the highest stabilized PCE (sPCE) of 1.7%. and greater phase stability of the α - CsPbI_3 .^[16] From XRD data, it was suggested that the greater phase stability was caused by strain in the crystals. Luo et al. developed a novel phase-transition scheme to fabricate α - CsPbI_3 solar cells from Cs_4PbI_6 by IPA treatment to increase the sPCE to 1.9%.^[92] Ripolles et al. reported a rfPCE of 4.2% using a thin layer of MoO_3 between the hole-transport medium (HTM) and Au contact which reduced hysteresis.^[93] Hutter et al. used vacuum-based vapor deposition of alternating very thin layers of CsI and PbI_2 and obtained a sPCE of 7.8% compared to 4.3% for spin-coated CsPbI_3 . The main improvement in vapor-deposited HaP properties was the much longer carrier lifetimes ($>10\ \mu\text{s}$) compared to the spin-coated samples and presumed lower trap densities.^[49] Yonezawa et al. used sequential evaporation and reported 5.7% reverse scan PCE.^[94] Frolova et al. used co-evaporation of CsI and PbI_2 and reached a rfPCE of 9.9%.^[95] Figure S6 in the Supporting Information of that paper also shows a stability plot over about 30 min of cell operation showing a $\approx 7\%$ current drop over load (near maximum power) within several seconds (equivalent to ca. 14% PCE drop), followed by complete stability for the rest of the time: this is longer than usually given for CsPbI_3 . Most recently, You et al. reported a rfPCE of 15.3% (certified efficiency of 14.67%) by waiting some tens of minutes after spin-coating before annealing, which allowed a partial phase change to occur in this time.^[95] Hysteresis was smaller than usual in these cells. The annealed CsPbI_3 was stable for over 2 months in N_2 . Light saturation of the cells under N_2 (presumed under open circuit conditions) showed relatively good (for this material) PCE stability with a small increase over a few days followed by a slow decrease (at a rate of ca. 0.5% day $^{-1}$). Xiang et al. reported that stable α - CsPbI_3 can be obtained by replacing PbI_2 with HPbI_3 in a one-step deposition.^[96] The E_g of the CsPbI_3 was reduced from 1.72 to 1.68 eV, suggested due to the existence of tensile lattice strain. By employing such α - CsPbI_3 films in cells using carbon as a direct contact to the HaP (no HTM), a reverse-scan PCE of 9.5% was achieved. The cells were stable when stored in dry (10–20% RH) air for around 4 months, showing the high

stability. It was also noted that the grain size of the films was approximately 320 nm, meaning that the stability was not due to a small crystal size as had been found in other studies. The values of the open circuit voltage (V_{OC}) for all the above cells varied from well under 1.0 V to a maximum of around 1.1 V.

While recent improvements in phase (and therefore cell) stability are promising, it is clear that improvements in stability, in particular phase stability, are needed. There are several directions by which this can be done:^[97]

- 1) Lower-symmetry perovskite orthorhombic black phases ($\beta\text{-CsPbI}_3$ and $\gamma\text{-CsPbI}_3$).
- 2) Reducing crystal size or dimensionality (quantum dots, mixed 2D/3D systems).
- 3) Adsorption/surface reaction of organic compounds.
- 4) Partial substitution of the Pb-site cations with smaller ions.

We separate these different strategies into groups below but note that often, it would be possible to put a specific study into more than one group.

4.1.1. Disordered Metastable Black Phase

In Section 2.1, we discussed the different known phases of CsPbI_3 : the non-perovskite (and PV-almost inactive) δ -yellow phase and the three black perovskite phases: α -

(cubic), β - (tetragonal), and γ - (orthorhombic) in order of increasing octahedral tilting. The room-temperature thermodynamically stable phase converts into the undistorted $\alpha\text{-CsPbI}_3$ at approximately 360°C; upon cooling, this phase transitions through the β -phase at 260°C and the γ -phase at 175°C with decreasing I-Pb-I angle.^[46] The band gaps of the α -phase (1.73 eV) and γ -phase (1.67 eV) are close—the α -phase might be a little better for a Si tandem cell while the γ -phase would be slightly better for a single-junction cell.^[98]

Fu et al. deposited orthorhombic CsPbI_3 in a one-step spin-coating film deposition by using phenylethylammonium (PEA) iodide (shown in Figure 4a). In contrast to the 2D/3D materials (see below), the concentration of PEA was much higher ($\times 2$ the Cs concentration), while apparently maintaining the orthorhombic phase without evidence of layering. The films were phase-stable over four months in air, which is believed to be due to capping of the CsPbI_3 crystals by the bulky organics. A cell PCE of 6.5% with V_{OC} of 1.06 V was reported.^[30] Zhao et al. described formation of orthorhombic $\gamma\text{-CsPbI}_3$ films with intrinsic thermodynamic stability by adding a small amount of water (in addition to the water in the HI also added).^[99] It was suggested that the added water affects ionization in the precursor solution (shown in Figure 4b) leading to the γ -phase and also a smaller crystal size. Theoretical calculations showed that $\gamma\text{-CsPbI}_3$ has a lower

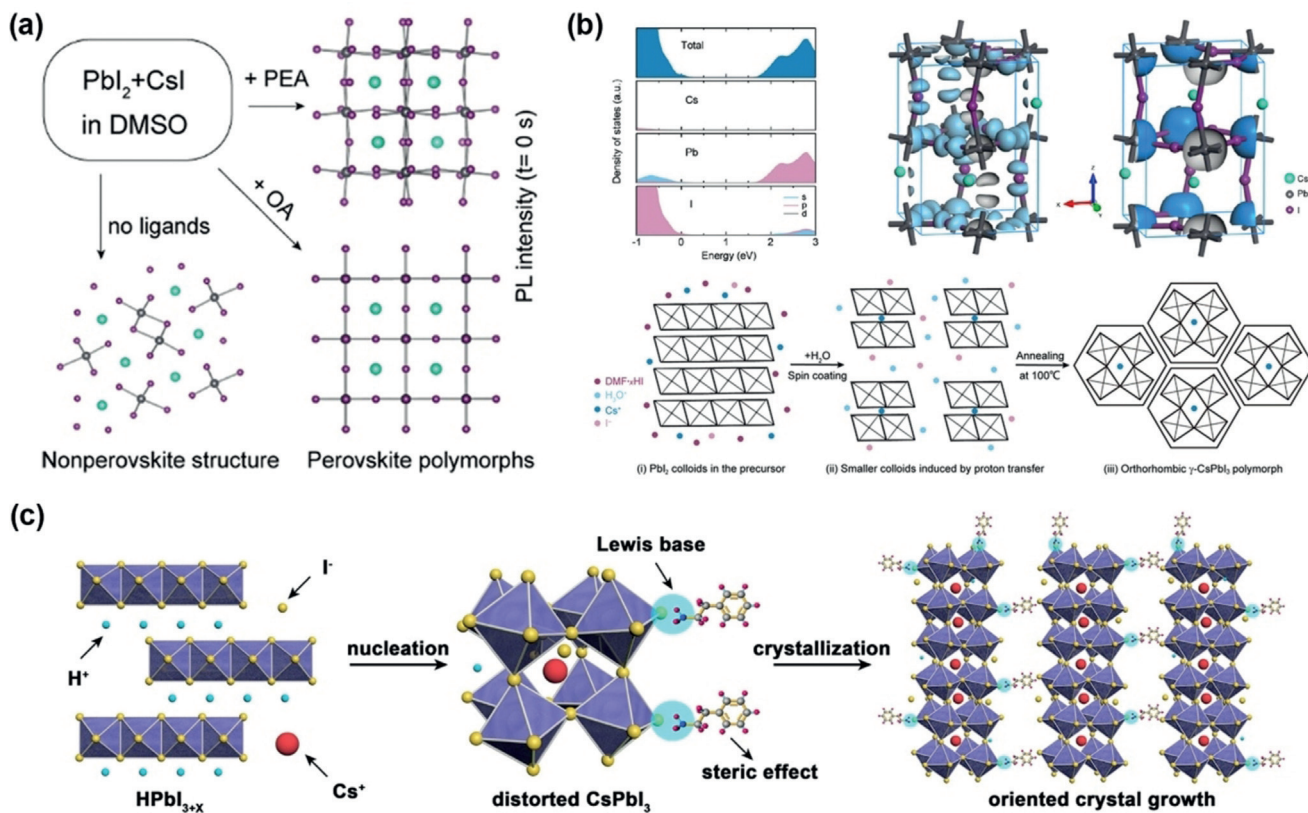


Figure 4. a) Schematic illustration of hypothesized surface ligand functionalization of the CsPbI_3 structures, $\delta\text{-CsPbI}_3$ without surface ligands, OA-stabilized $\alpha\text{-CsPbI}_3$, and PEA-stabilized $\gamma\text{-CsPbI}_3$. Reproduced with permission.^[30] Copyright 2017, American Chemical Society Publications. b) Optoelectronic properties and scheme for the stabilization of $\gamma\text{-CsPbI}_3$. Reproduced with permission.^[99] Copyright 2018, American Chemical Society Publications. c) Schematic for HI and PEAI additive-induced $\gamma\text{-CsPbI}_3$ crystal growth. Reproduced with permission.^[101] Copyright 2018, Nature Publishing Group.

surface free energy than the yellow δ -phase. E_g was approximately 1.75 eV, very close to that of the α -phase. The γ -CsPbI₃-based PSCs displayed a sPCE of 9.7% (stable over two hours of cell operation) and 11.3% reverse scan PCE with reverse scan $V_{OC} = 1.04$ V. The films were stable in ambient air (10% RH) for a month. In the same study, they obtained β -CsPbI₃ (tetragonal) in the absence of HI and water after annealing at 330°C and cooling. However, this phase was much less stable to ambient conditions than the γ -phase. It is worth noting that polar ethanol treatment of α -CsPbI₃ nanocubes (ca. 20 nm) was shown to result in their conversion into γ -CsPbI₃ as well as self-assembly into strings.^[100]

Wang et al. fabricated distorted black phase (lower-symmetry orthorhombic) CsPbI₃ film via the synergistic effects between HI and PEAI additives.^[101–104] HI induces intermediate HPbI_{3+x}, leading to the formation of a stabilized distorted black phase with $E_g = 1.69$ eV. As shown in Figure 4c, the PEAI⁺ is physically absorbed on the surface of CsPbI₃ and functions chemically in the formation and stabilization of CsPbI₃ through the C–N bond in PEAI⁺. Hence, PEAI plays a dominant role in the nucleation and growth of the CsPbI₃ film. It also stabilizes the distorted black phase by hindering phase transition through its steric effects. By optimizing the annealing process, the corresponding solar cell achieved a sPCE of 15.1% and V_{OC} of 1.06 V. The stability was very high and much better than the same cell without the PEAI addition.

4.1.2. Reducing Crystal Size/Dimensional Engineering

The size-dependent phase diagrams suggest that the cubic phase becomes more stable when the nanocrystal size or dimension is decreased.^[105]

4.1.2.1. QD Films

Highly crystalline CsPbI₃ QDs enable solution processing and are a powerful platform for tuning optical and electrical properties useful for optoelectronic devices.^[106,107] However, in the case of CsPbI₃, the most important attribute of quantum dot films is their greater phase stability when pure, compared to polycrystalline films (months in ambient air) as described by Swarnkar et al.^[85] This can probably be related to the greater phase stability of α -CsPbI₃ in colloidal quantum dots^[36] and in small-crystal polycrystalline films discussed above.^[106] This seems to be a function of crystal size rather than having any connection with size quantization. In fact, all the work up to now on CsPbI₃ QDs used QDs between 10 and 30 nm and which showed only very small (if any) increase in E_g . Therefore it is probably more correct to consider the semiconductor as nanocrystals in general rather than as quantum dots, although we will continue to use the term QD herein as this is how most of the authors refer to them.

Swarnkar et al. reported a device (shown in Figure 5a) based on α -CsPbI₃ quantum dot films with a reverse bias PCE of 10.8%.^[85] The QDs were purified to remove the long oleate ligands (that would prevent charge transfer between QDs) which were exchanged with short MeOAc ligands (some

ligand is needed to prevent agglomeration of the QDs). This solar cell remained stable for two months in a dry, dark environment with no loss of PCE. It had a large V_{OC} of up to 1.23 V (for an $E_g = 1.75$ eV, only slightly higher than the normal, non-quantized value of 1.73 eV). Wang et al. used μ -graphene (μ GR) to crosslink QDs to form a μ GR/CsPbI₃ composite film (shown in Figure 5b).^[86] It was found that the resultant QD film provides an effective channel for carrier transport, as witnessed by much improved conductivity. The best reverse PCE was 11.4% compared to 10.4% without μ GR—a 12% increase. Again, high values of V_{OC} up to 1.18 V ($E_g \approx 1.75$ eV) were obtained. In addition, it also shows significantly better stability against moisture and high temperature stress. The instability originating from the thermal/moisture-induced QD agglomeration, which leads to phase change, was also greatly suppressed by the μ GR crosslinking.

Sanehira et al. developed QD films with tuned surface chemistry based on variation of the A-site cation halide salt (AX; Figure 5c). FAI gives the best results. The AX treatments provide a method for tuning the coupling between perovskite QDs, leading to improved charge transport, seen as an increase in mobility, for fabricating high-quality QD films. They reported a certified QD PSC efficiency of 13.43% with V_{OC} up to 1.22 V.^[108] More recently, the same group described the mechanism of the ligand-exchange procedures through substitutes the long-chain oleate and oylamine cations by smaller FA cations (shown in Figure 5d,e).^[109] The most common HTM in CsPbI₃ cells is spiro-OMeTAD (spiro). In Ref. [86] PTAA (polytriarylamine) was used. Yuan et al. looked at several different polymeric HTMs for CsPbI₃ QD PSCs to avoid potential effects of the dopants used in spiro on the quantum dots.^[110] Three different HTMs were used and were all superior to spiro, both in terms of PCE and in reduced hysteresis. Besides efficiencies approaching 13% (there was little difference between forward and reverse scans), a record high V_{OC} of up to 1.28 V was reported. Since E_g was measured to be 1.73 eV, this translated into a very low voltage loss of 0.45 V.

We finish this Section by referring to a recent report by Dutta et al. who prepared CsPbI₃ nanocrystals at a higher than usual temperature (260°C) and with oleylamine (OLA) and HI in the reaction mixture. They reported that the stability of the (ca. 15 nm) nanocrystals in the α -phase was higher for these nanocrystals than if the nanocrystal preparation were carried out at a more usual temperature (160°C).^[111] From NMR experiments, they explained this by stronger binding of OLA⁺ to the higher-temperature-prepared nanocrystals. Such success in CsPbI₃ nanocrystals gives us inspiration which could lead to record-breaking performance in QDs solar cell in the future.

4.1.2.2. Mixed 2D/3D Films

In contrast to the three-dimensional (3D) counterparts, layered 2D HaP films are made up of one octahedral layer connected in two dimensions and separated in the third dimension by a large organic cation. They show much increased stability compared to normal 3D HaPs, probably due to capping by the large cations and van der Waals

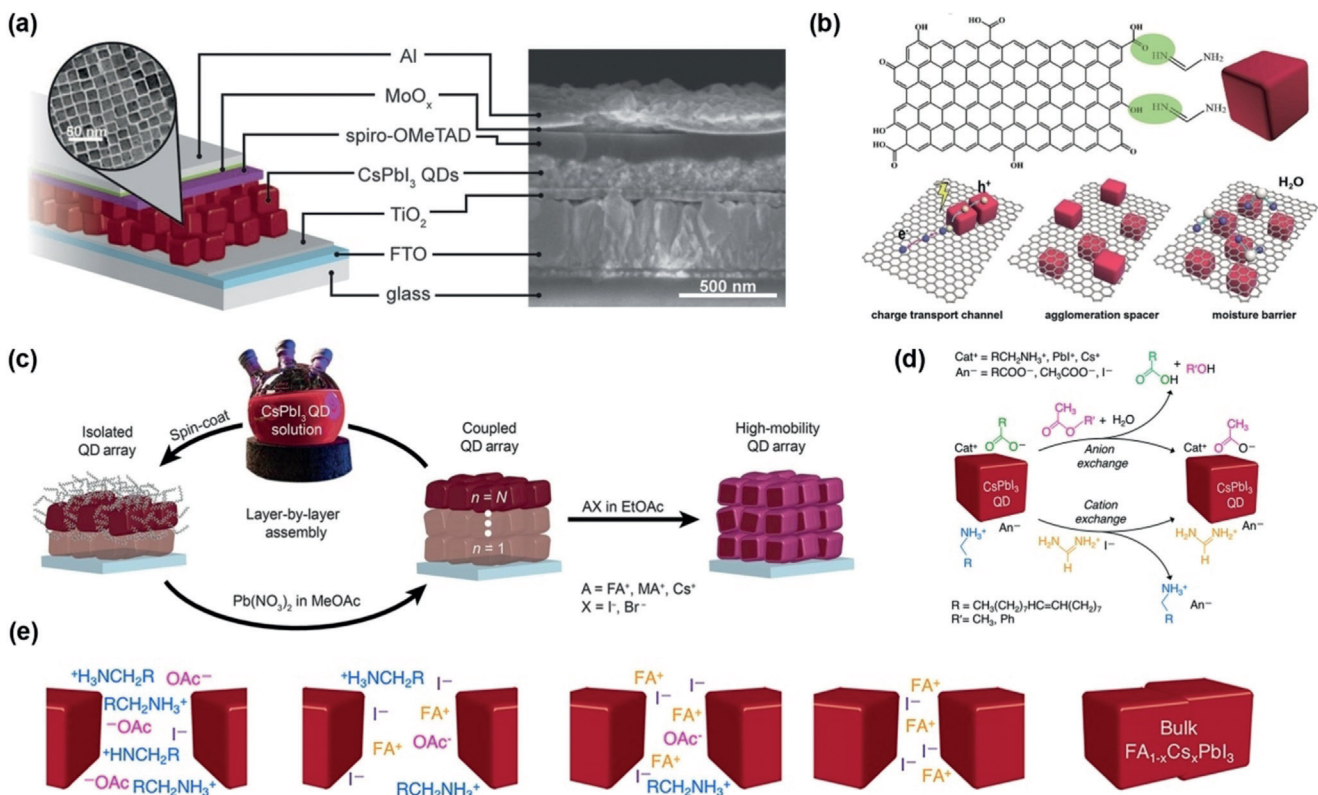


Figure 5. a) Schematic and SEM cross-section of the CsPbI_3 PSCs. Reproduced with permission.^[85] Copyright 2016, Science Publishing Group. b) Chemical structure of the μGR and CsPbI_3 QDs, and their crosslink mechanism; schematic drawing of the charge transport process and stabilization mechanism for the $\mu\text{GR}/\text{CsPbI}_3$ film based PSCs. Reproduced with permission.^[86] Copyright 2018, Wiley-VCH Publications. c) Schematic of QD CsPbI_3 film deposition process with AX salt post-treatment. Reproduced with permission.^[108] Copyright 2017, Science Publishing Group. d) Anionic carboxylate ligand-exchange and cationic ligand exchange reaction in CsPbI_3 thin films and e) schematic representation of surface composition of CsPbI_3 QD films. Reproduced with permission.^[109] Copyright 2018, American Chemical Society Publications.

interactions between the cations which form a good blocking layer to water.^[112] However, they have several disadvantages compared to the 3D HaPs related to their much lower dielectric constants (therefore large exciton binding energies and poor screening of eh^{-1} recombination), as well as poor charge transfer unless the 2D sheets are perpendicular to the substrate. However, by adding a small amount of large cation (typically ca. 10% of the total A cation), a mixture of 3D HaP separated by large cations is formed and known as 2D/3D materials. Therefore by tailoring n , properties lying between those of pure 3D HaPs ($n \rightarrow \infty$) and pure 2D ($n = 1$) can be obtained, in particular improved stability with only a small drop in the dielectric constant from pure 3D.

Although containing a large proportion of an organic cation, it is worth mentioning that Liao et al. combined a butyl ammonium (BA) cation with Cs^+ to give the stoichiometric composition $\text{BA}_2\text{CsPbI}_7$ which appears to form as sheets of two corner-connected octahedra in two dimensions separated from similar sheets by the BA cations. The XRD pattern of this material is very similar to that of $\alpha\text{-CsPbI}_3$ (and very different than that of pure BA_2PbI_4) except for a strong preferential orientation of the structure perpendicular to the substrate (i.e., charge transfer does not need to

go through the BA links). A PCE of 4.8 % was reached with a drop of only 9 % after 5 days illumination (presumed open circuit conditions).^[113] Phenylethylammonium (PEA) is becoming a popular cation in 2D/3D HaPs and was used by Li et al. to modify CsPbI_3 .^[114] For $\text{Cs}_{0.9}\text{PEA}_{0.1}\text{PbI}_3$, they obtained a sPCE of 5.6 % with little hysteresis and after storing an unencapsulated cell in a dry box for 95 h, it retained 75 % of the PCE. Jiang et al. also introduced PEAI into CsPbI_3 to induce formation of a 2D/3D HaP^[115] (shown in Figure 6a). The resulting HaP exhibited significantly suppressed phase transition, a reduced trap density and a sPCE of 12.2 % and $V_{\text{OC}} = 1.07$ V. They also adopted a new precursor pair, cesium acetate (CsAc) and hydrogen lead trihalide (HPbX_3), by which they were able to overcome the notorious solubility limitation for Cs precursors to fabricate high-quality CsPbX_3 perovskite films with film thickness up to 500 nm. Zhang et al. added ethylenediamine (EDA) dications which helped stabilize the black $\alpha\text{-CsPbI}_3$ phase and also gave smaller-sized crystals (from ca. 300 nm without EDA to ca. 35 nm with 2.5% EDA) and fewer pinholes, making it possible to attain 10.5 % sPCE, $V_{\text{OC}} = 1.15$ V ($E_g \approx 1.73$ eV) with dark, dry box-storage stability for months at room temperature.^[116]

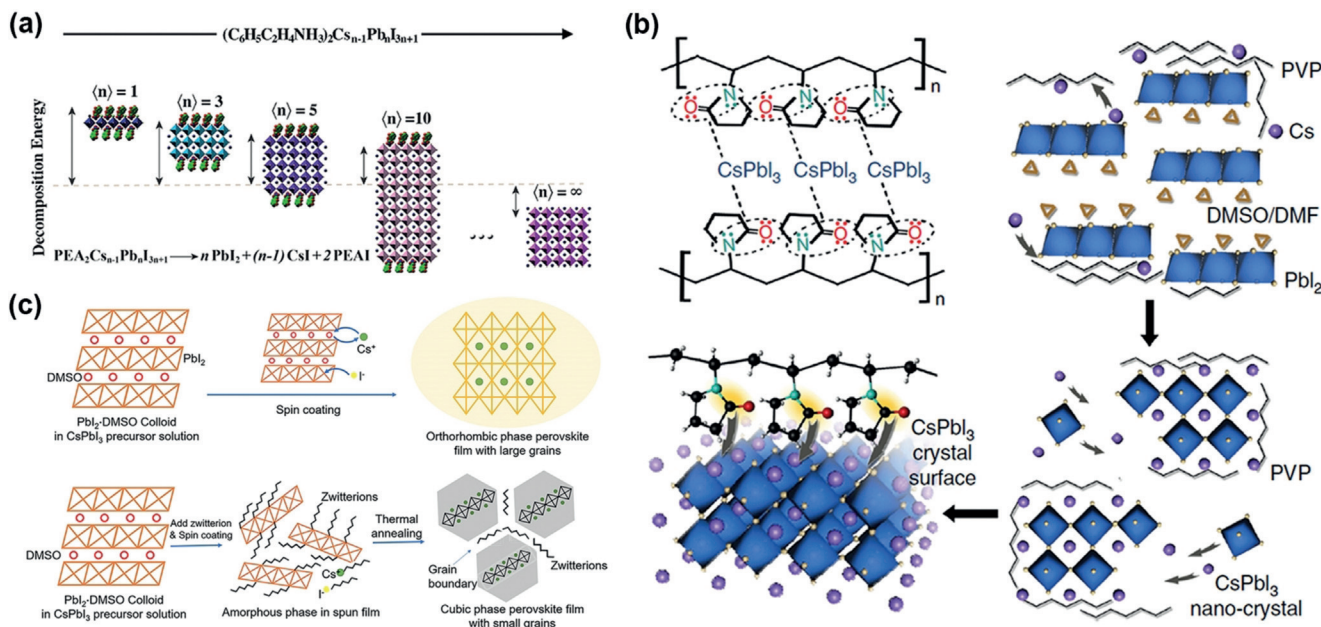


Figure 6. a) Structure of $\text{PEA}_2\text{Cs}_{n-1}\text{PbnX}_{3n+1}$ with different n values. Reproduced with permission.^[115] Copyright 2018, Elsevier Inc Publications. b) Mechanism of PVP-induced cubic phase stability of CsPbI_3 PSCs. Reproduced with permission.^[117] Copyright 2018, Nature Publishing Group. c) Mechanism of CsPbI_3 α -phase stabilization by Zwitterion. Reproduced with permission.^[119] Copyright 2017, Elsevier Inc Publications.

4.1.3. Organic Modification

There are a number of studies describing the effects of adsorption of organic species on CsPbI_3 crystal surfaces with the main reason being to stabilize one of the black phases. Other effects of such adsorption are reduction in crystal size (which may be the cause, in part or in whole for the stabilization) or passivation of surface traps. Different organic species have been used for this purpose: polyvinylpyrrolidone (PVP, shown in Figure 6b),^[117] polyethylene oxide (PEO),^[118] sulfobetaine zwitterions (shown in Figure 6c),^[119] phenyltrimethylammonium bromide (PTABr),^[17] phenylethylammonium cation (PEA)^[120] and diethylenetriamine (DETA).^[121] In all but Refs. [17, 120], the overall result seems to be similar—the large organic species suppresses crystallization of the HaP and results in much smaller crystal size, which assists stabilization of the black-phases. In fact, in the case of the zwitterions,^[119] the as-deposited CsPbI_3 is either XRD amorphous or of very small grain size (no more than a few nm), which grew to approximately 30 nm after annealing. In Refs. [17, 63], the treatment was after CsPbI_3 deposition and, as expected, there was no change in crystal size, yet the treatment increased the phase stability. Therefore it is reasonable to assume that both crystal size and surface functionalization preventing water reaching the HaP play a role in stabilizing the black phase. In Ref. [121], the importance of surface functionalization to “lock” the cubic structure as well as increased hydrophobicity to prevent water vapor access to the HaP were considered to be important as well as the decrease in crystal size.

The organic species increased the charge lifetimes^[117, 118] as well as cell performance.^[120, 121] In the PTABr treatment, some Br/I exchange occurred, giving a graded junction, which also might have an effect on phase stability: however the amount

of Br in the films was very small, giving a spectral blue shift of under 5 nm (equivalent to less than 2% of the total halide based on a homogeneous HaP).^[17] The PCEs of cells reported in these studies (Ref. [118] dealt with LEDs) were mostly high, with $V_{OC} \approx 1.1$ V in all cases and PCEs of 10.6%,^[117] 11.4%,^[119] 13.5%,^[120] 6.8%^[121] and 16.3%,^[17] all stabilized PCEs except for Refs. [117, 121] which were rfPCE.

4.1.4. Ionic Incorporation

A different strategy to improving the stability of α - CsPbI_3 is to increase the Goldschmidt tolerance factor (see Section 2.1) by partially exchanging the B atom (Pb). The most obvious candidate for this is Sn, which is smaller than Pb. While Sn HaPs have a well-known problem of instability because of oxidation of Sn^{II} to Sn^{IV} , solid solutions of Pb-Sn HaPs are quite stable if the Sn content is not too high. The only study we are aware of that alloys some Sn with CsPbI_3 is on QDs (ca. 15 nm) with varying amounts of Sn, but with emphasis on 60% Sn, 40% Pb.^[122] The mixed Pb/Sn QDs were considerably more stable in air than pure CsPbI_3 , even in the absence of capping ligands. The crystal structure was different than QDs of cubic CsPbI_3 , and seems to be the (black) orthorhombic phase (compare with the apparently stable γ -orthorhombic phase discussed earlier).^[99] Hu et al. introduced Bi^{3+} which is a little smaller than Pb^{2+} and found much greater stability in air (55% RH) compared to the same material without Bi.^[123] Besides the expected increase in tolerance factor, the Bi-incorporation resulted in smaller grain size and increased microstrain in the crystals, both of which could also play a role in increasing stability. Using CuI as an inorganic HTM, they obtained (for 4 at % Bi^{3+}) a sPCE of 13.2% and V_{OC} of 0.97 V; the apparent E_g also decreased to 1.56 eV which explains the lower V_{OC} (for CsPbI_3) than usual for good

cells. Recently, they fabricated flexible solar cells based on such films with sPCE of 10.8%.^[124] Lau et al. reported the addition of Ca²⁺ (optimum ca. 5 at % of Pb) to the CsPbI₃ with a modest improvement in stability.^[125] In this case, the grain size of the HaP increased and no strain was invoked. The cells were good with sPCE = 13.3% ($V_{OC} = 0.95$ V). The main role of the calcium seems to have been surface/grain boundary passivation by Ca–O species rather than incorporation of Ca into the lattice. Other studies looked at incorporation of Sb³⁺^[126] and Eu³⁺ (believed to be mainly interstitial)^[127] into CsPbI₃. Reduction in grain size (more pronounced in Ref. [127] and lattice strain was invoked in both to explain improved stability. Ref. [126] also noted that excess of CsI in the preparation solution also led to reduced grain size and increased stability. In both cases, the cell efficiencies were modest (ca. 5%). Finally, we mention Mn doping of CsPbI₃ nanocrystals (12 nm) described by Akkerman et al. where substitution of 10% of the Pb by Mn increased the α -CsPbI₃ stability by approximately 40 times due both to the increased tolerance factor and calculated increase in cohesive energy.^[128]

4.2. CsPbBr₃ PSCs

CsPbBr₃ has a wide E_g (ca. 2.3 eV), which is a bit high for most PV use, except possibly for multi-tandem cells (e.g. a four-stage tandem).^[129–131] However, by mixing with I (to be discussed below), it can be very useful for simpler tandem cells. The solution-based deposition methods typically used for CsPbX₃ are difficult to directly adapt for CsPbBr₃, owing to the lower solubility of CsBr precursors in commonly used deposition solvents.^[132,133] In contrast to CsPbI₃, CsPbBr₃ is stable in the orthorhombic structure at and near room temperature;^[134] for that reason, in contrast to our emphasis on phase stability in the previous section on CsPbI₃, the emphasis in this section will be more focused on PV properties. We divide this Section up according to the methods mainly used to prepare CsPbBr₃—two-step solution method, vacuum deposition method, and quantum dot method.

4.2.1. Two-step Solution Method

In 2015, Kulbak et al. first reported CsPbBr₃ PSCs with the aim of answering the question: is the organic A cation necessary for the high PCE and V_{OC} obtained in hybrid HaP cells. With a rfPCE of 5.8% and V_{OC} of 1.28 V, they showed that the organic cation was not essential, although it does seem at the moment that the hybrid HaPs do have a small (typically 100–150 mV) advantage in V_{OC} .^[15] The same group also showed the higher stability of CsPbBr₃ compared to MAPbBr₃ to heat, e-beam and as cells.^[60] Liang et al. used carbon as a contact to a HTM-free cell.^[135] A PCE of 6.7% with $V_{OC} = 1.24$ V was reported. The (storage) stability of these cells, without encapsulation, was excellent; they showed no degradation of PCE in humid air (90–95% RH, 25°C) for over 3 months and could endure both extreme temperatures (100°C) and temperature cycling (−22 to +100°C) for long periods without loss of PCE. Adding Cl[−] ions is well-known to

improve hybrid HaP cells, including the morphology of the HaP films. Li et al. developed a Cl[−] “doped” CsPbBr₃ absorber with cubic structure to achieve a PCE as high as 6.2% although with a lower than usual V_{OC} (1.02 V).^[136] The improvement of photovoltaic performance compared to Cl-free HaP could be attributed to enhanced carrier lifetime, diffusion length and extraction rates, as well as suppressed nonradiative recombination.

Duan et al. used a multi-step method of converting PbBr₂ into CsPbBr₃ by spin-coating CsBr solution onto the PbI₂ in several steps (shown in Figure 7a).^[77] While the specific phase and composition was strongly dependent on the number of steps, using four steps gave CsPbBr₃ with large (>1 μm) grains and cells (carbon contacts directly to the HaP) of 7.1% sPCE and V_{OC} of 1.308 V. By depositing graphene nanoparticles on the TiO₂ electron transporting layer (ETL), they apparently reduced the electron affinity of the TiO₂ and thus also the mismatch between the HaP and TiO₂ conduction bands, reporting a sPCE of 9.6% with $V_{OC} = 1.458$ V. The same group, using the same system except with the addition of ZnS-capped CuInS₂ QDs between the CsPbBr₃ and carbon electrode, reached a sPCE of 9.4% and V_{OC} of 1.522 V (the CuInS₂:ZnS QDs did not contribute to the photocurrent).^[137] In this case, water vapor in the carbon supposedly dissociated to H⁺ forming a double layer at the carbon surface and was believed to add to the overall conversion (probably mainly through increase in the V_{OC}). It is not clear how the same cell would operate in the absence of water. It is noteworthy that, over 40 days storage at 80% RH without encapsulation, only a few % loss occurred in PCE. The efficiency of cells made using this multi-step method and with carbon contact to the HaP (without either graphene or CIS:ZnS nanoparticles) could be further increased using alkali metal substituents for the A cation^[78] or lanthanide substituents for the Pb.^[138] They reported 9.8% sPCE and 1.552 V V_{OC} for 9% Rb substitution, and 10.1% sPCE and 1.594 V V_{OC} for 3% Sm substitution. Storage stabilities were also very high—for unencapsulated Sm⁺-“doped” cells, essentially no drop after 110 days at 80% RH and the same for dry storage at 80°C, also for 110 days (the same cell without Sm dropped about 15% in PCE after the same time). We note CsPbBr₃ cells made using PEABr, CsAc, and HPbBr₃ have been reported with 6.5% PCE and 1.26 V.^[115]

4.2.2. Vacuum Deposition Methods

Luchkin et al. demonstrated that thermal ageing of evaporated CsPbBr₃ films increased the photocurrent and V_{OC} and explained this by downwards band bending at the grain boundaries leading to better electron–hole separation.^[139] An average PCE of 3.9% and V_{OC} of 0.94 V was obtained. Lei et al. through systematic optimization of the deposition parameters with dual-source vacuum evaporation, obtained CsPbBr₃ films with good crystallinity and uniformity at an optimum annealing temperature of 500°C (with the film covered by glass in N₂ to minimize vaporization loss). PSCs with rfPCEs of 6.7% and $V_{OC} = 1.27$ V were obtained for small (0.09 cm²) cells and 5.1% and $V_{OC} = 1.315$ V for larger (1 cm²) cells.^[89] The appreciably larger V_{OC} for the larger cells

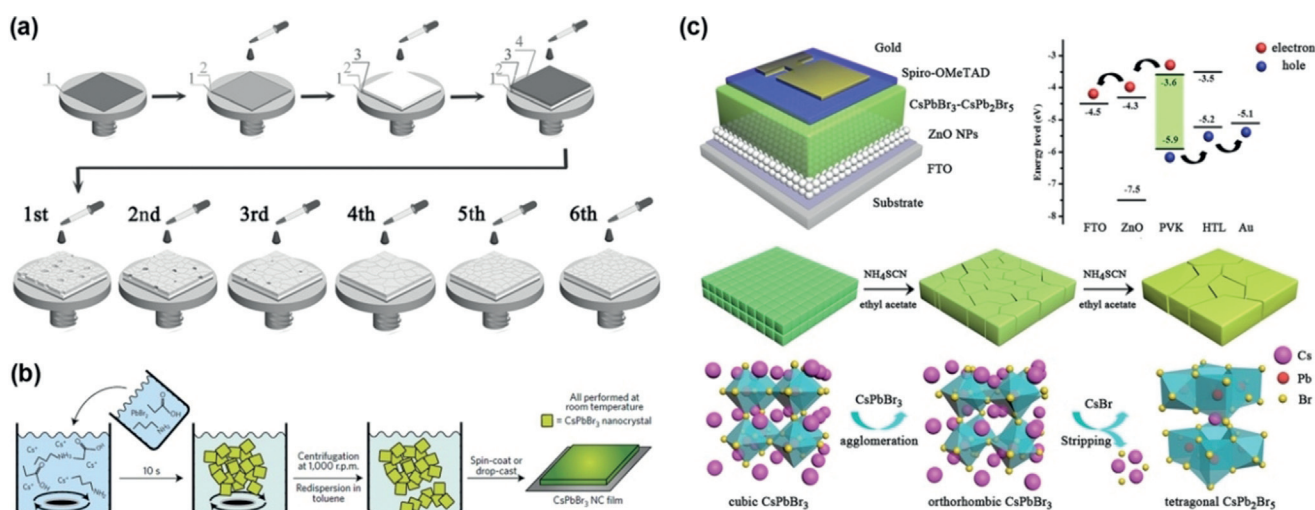


Figure 7. a) Illustration of multistep solution-processed deposition of CsPbBr_3 process. Reproduced with permission.^[77] Copyright 2018, Wiley-VCH Publications. b) Schematic method of the CsPbBr_3 QDs passivated with short ligands. Reproduced with permission.^[74] Copyright 2016, Nature Publishing Group. c) Schematic structure and energy level diagram of the CsPbBr_3 – CsPb_2Br_5 device, the film fabrication process and the phase transformation mechanism (from cubic CsPbBr_3 to tetragonal CsPb_2Br_5). Reproduced with permission.^[82] Copyright 2018, American Chemical Society Publications.

is interesting but more statistics would be needed before reading any meaning into this.

Li et al. introduced some CsPb_2Br_5 into CsPbBr_3 using a small excess of PbBr_2 relative to CsBr .^[140] The presence of CsPb_2Br_5 at the CsPbBr_3 grain boundaries passivated grain defects and reduced the carrier recombination. 7.6% rfPCE with $V_{OC}=1.29\text{ V}$ were reported. Chen et al. studied transparent CsPbBr_3 cells for use in tandems.^[141] Slow evaporation (0.5 nm s^{-1}) gave the largest crystal size (several 100 nm to over 1 μm). Non-transparent cells gave a reverse PCE = 7.8%, $V_{OC}=1.44\text{ V}$, while transparent cells (on PEDOT/PSS as contact) gave 6.0% and 1.38 V.

4.2.3. Quantum Dot Methods

Akerman et al. developed room-temperature-prepared CsPbBr_3 nanocrystal (15–20 nm) inks to fabricate fully air-processed PSCs exhibiting PCE exceeding 5% with $V_{OC}=1.5\text{ V}$ (Figure 7b).^[74] Butylamine ligands were used that remained when the spin-coated inks were processed into cells; they apparently were short enough (or possibly also sparse enough) so as not to impede charge transfer but did act to passivate the nanocrystal surfaces. This method provides an interesting pathway for large-scale fabrication of HaP devices. Panigrahi et al. used conventional hot-injection to prepare CsPbBr_3 nanocrystals and fabricated cells with 4.2% PCE and 0.86 V.^[142] The emphasis in that investigation was to study the charge distribution in the cells. They found an unbalanced charge separation in the HaP with hole accumulation leading to barrier formation.

Hoffman et al. developed a layer-by-layer methodology of CsPbBr_3 QD deposition with subsequent annealing at 250°C to cast stable films of a desired thickness.^[132] Devices optimized to both QD spin-casting concentration and overall CsPbBr_3 thickness produced devices of 5.5% PCE and $V_{OC}>$

1.4 V with very little hysteresis. Recently, Zhang et al. fabricated nanocrystal (10–20 nm) films and processed them using NH_4SCN in ethyl acetate solution to transform the CsPbBr_3 film into a CsPbBr_3 – CsPb_2Br_5 composite film (shown in Figure 7c) with larger crystal size which resulted from the dissolution/recrystallization by the treatment. The small amount of CsPb_2Br_5 in the composite film resulted in surface passivation of CsPbBr_3 by decreasing the number of Br vacancies at the Br-enriched surface. Cells fabricated from these films gave a rfPCE of 6.7% and V_{OC} of 1.435 V.^[82]

4.3. CsPbBr_2I PSCs

Incorporation of iodine into CsPbBr_3 as CsPbBr_2I leads to decreased E_g (ca. 2.05 eV).^[143,144] However, it was shown that for $\text{CsPb}(\text{Br}_{x}\text{I}_{1-x})_3$, for $x > 0.4$, the system phase-segregates into I- and Br-rich phases upon illumination.^[145] Li et al. also found that CsPbBr_2I was prone to segregation.^[146] They found that under illumination, “iodide-rich” $\text{CsPbBr}_{(2-x)}\text{I}_{(1+x)}$ phases form at grain boundaries as well as segregate as clusters inside the film. Phase segregation generates a high density of mobile ions moving along grain boundaries as ion migration “highways”. Finally, these mobile ions pile up at the perovskite/ TiO_2 interface resulting in formation of larger injection barriers, hampering electron extraction and leading to strong J - V hysteresis in CsPbBr_2I -based PSCs. At the same time, Ma et al. did not find such segregation in their CsPbBr_2I films.^[147] In contrast to the previous solution-formed films, the ones prepared by Ma et al. were deposited by vacuum evaporation. Among other studies on this HaP, Lau et al., using spray deposition, do not mention segregation,^[148] and Liu et al. report no phase separation occurs in their films, although it is not clear if this refers only to non-illuminated films.^[149] In fact, in their (inverted) cells, there is a rapid drop

in PCE of nearly 40% in the first 10 s during illumination which might be due to light-induced segregation (although it could also be due to other factors). Of particular importance is a recent study by Zhu et al. in which they used a CsI treatment of their films to fabricate large (typically 0.6 µm) and textured grains which did not exhibit segregation, in contrast to the same films without the CsI treatment, which did phase-segregate.^[150] We can conclude from combining all these studies that, while phase segregation may occur, it does seem to depend on the specific films involved and how they were fabricated.

4.3.1. Performance-Optimized Cells

The earliest study on CsPbIBr₂ cells seems to have been by Ma et al. who used vacuum deposition and achieved a rfPCE of 4.2% and rfV_{OC} of 0.89 V with a large hysteresis.^[147] The same group later used spray-pyrolysis to deposit the films and obtained a sPCE of 6.3% and V_{OC} of 1.12 V with almost no hysteresis.^[148] In fact, with the exception of this study and, to some extent Ref. [150], which showed a moderate hysteresis, all the other J-V curves for this material exhibited major hysteresis. Li et al. obtained a sPCE of 6.1% and rfV_{OC} = 1.20 V.^[146] Liu et al. used an unusual inverted cell structure with NiO as HTM and Au evaporated on a 4 nm thick MoO_{3-x} buffer layer on the HaP.^[149] Note that the Au/MoO₃ contact was the electron-extraction contact and not the hole-extraction contact as is usually the case; the work function of the MoO_{3-x} was measured to be 4.3 eV, and was deliberately reduced to give a lower work function than usual. They obtained approximately 3% sPCE with V_{OC} < 850 mV. The most recent study by Zhu et al. using their CsI treatment mentioned above that resulted in large crystal size, gave 8.5% sPCE with rfV_{OC} = 1.21 V. We briefly also note that CsPbIBr₂ has been used in a transparent cell as a thermochromic window: exposed to moisture, it becomes pale yellow and very transparent while above 105°C it converts reversibly back into the deep orange HaP with a sPCE of 5.1%.^[151] Finally, using PEA incorporation together with CsAc and HPbX₃, Jiang reported 9.5% PCE and 1.19 V.^[115]

4.3.2. Ionic Incorporation

Liang et al. doped Mn (optimum 0.5% of the Pb) into CsPbBr₃.^[11] The Mn-doped films shows better crystallinity and morphology and a slightly decreased E_g (1.85 eV instead of 1.89 eV in the absence of Mn—itself considerably lower than the more usual ca. 2.0 eV for this HaP). PSCs, with carbon contacts to the HaP, showed a PCE of 7.4% (not specified how measured) and approximately 0.99 V V_{OC}. Another sample showed a sPCE of 6.7%.

There are two studies on solid solutions of Sn substituting for Pb in these CsPbBr₂I HaPs. One study describes CsPb_{0.9}Sn_{0.1}IBr₂ with a E_g of 1.79 (close to optimal for Si tandems).^[152] A (reverse scan) PCE of 11.3% was reported for cells using a carbon contact directly on the HaP. Based on the mild-to-moderate hysteresis in the cells, this probably translates to approximately 10.5% sPCE. The V_{OC} was about 1.25 V—a voltage loss of only 0.54 V which is low for such

a Br-rich material. Part of the reason for this might be the better energy level matching, mainly because of the lower E_g of the HaP. Very high storage stability was reported (no change in PCE of sealed cells after over 3 months). The other study varied the Sn content of a series of CsPb_{1-x}Sn_xBr₂I alloys and found an optimal Sn content for cells corresponding to CsPb_{0.75}Sn_{0.25}IBr₂ with E_g = 1.78 eV.^[153] This HaP exhibited a homogeneous and densely crystallized morphology. The cells showed an almost hysteresis-free PCE of 11.5% and V_{OC} = 1.21 V (another cell showed a sPCE of 11.1%). No segregation was found to occur and the stability was better than that of cells without Sn.

4.4. CsPbI₂Br PSCs

CsPbI₂Br, with a band gap of approximately 1.93 eV, is outside the composition range in which phase segregation is supposed to occur,^[145] although there is one study that does find such segregation.^[154] It is also more stable (in the black phase) against conversion into the yellow δ-phase compared to CsPbI₃ although it still can convert depending on the humidity level.^[155] It is much a more popular research topic than CsPbBr₂I, probably because of its more suitable band gap (it is ideal for triple tandems but may still be useful for double tandems). Hysteresis is very common in these cells and will be mentioned mainly where it was found to be very minimal. Because of this common hysteresis, it is even more important to give data as stabilized (sPCE) or rfPCE (or rfV_{OC}) where possible.

4.4.1. Stoichiometric Composition

We separate this Section on stoichiometric (or at least the absence of foreign atoms) HaP into the different techniques, mentioning only briefly details of the method where we consider them to be important as well as giving cell PCEs and V_{OC} and sometimes stability information.^[156] We note here that most cells are the standard TiO₂/HaP/spiro type, and there is limited work on alternate contacts or cell geometries.^[157]

Thermal evaporation methods: Ma et al. studied the effect of varying stoichiometry of CsPbI₂Br on film quality and cell performance.^[158] They found that CsBr-rich CsPbI₂Br is more stable to air exposure, while the stoichiometrically balanced CsPbI₂Br film gives the best photovoltaic performance (6.7% sPCE and V_{OC} ≈ 1.0 V). Chen et al. obtained sPCE = 11.5% and V_{OC} = 1.13 V with very little hysteresis and with superior device stability.^[159] They also measured operational cell stability (i.e. illuminated at ca. P_{max}) and found a less than 25% PCE drop after 120 h (note that most stability tests of these compounds are storage tests and not operational ones).

Two-step spin-coating method: Yu et al. deposited a composition which appears to be CsPb(Br_{0.43}I_{0.57})₃ by a two-step method using a MeOH/DMSO solution of CsBr, to increase its solubility, for the second step.^[84] A sPCE of 12.5% and high V_{OC} ≈ 1.33 V was obtained. Approximately 97% of the initial PCE was retained after storage for 480 h under ambient conditions.

One-step spin-coating deposition method: Nam et al. reported that the annealing conditions of CsPbI_2Br were very important for both solar cell efficiency and phase stability.^[160] They found 9.5% sPCE and 1.23 V V_{OC} for the optimized cell using a HaP layer only about 85 nm thick. Zhang et al. used a hot air flow over the spin-coated samples (DMF/DMSO solvent) for improved crystallization, and obtained cells with 11.1% sPCE and a maximum V_{OC} of 1.315 V.^[161] Another study also optimized DMSO concentration in mixed solvents with sPCE = 8.8% and $V_{\text{OC}} = 0.97$ V.^[162] This study showed operational stability data of less than 10% PCE loss after 500 h operating near P_{max} in N_2 (no UV in the illumination). Bai et al. found the precursor solution temperature strongly affected the crystallization process:^[75] to obtain thick film with large grain size, the precursor solution temperature was carefully adjusted (100°C was optimal) to both suppress the formation of too many nuclei and to increase the crystallization rate. Cells (made with PTAA HTM) showed 14.6% sPCE and 1.22 V V_{OC} (also a FF > 80%). Of particular importance, the cells showed almost no hysteresis.

Anti-solvent process: Dong et al. developed an effective anti-solvent process for fabricating high-quality inorganic HaP absorbers by using the less toxic, compared to most anti-solvents, ethyl acetate (EA).^[163] Compared with traditional spin-coating and widely employed chlorobenzene (CB) anti-solvent processes, the EA anti-solvent prepared CsPbI_2Br films exhibit improved surface morphology and larger grain size. The PSCs (carbon contacts to the HaP) based on EA-prepared CsPbI_2Br exhibited an rfPCE of 8.7% and $V_{\text{OC}} = 1.12$ V. Recently, Chen et al. precisely controlled CsPbI_2Br crystal growth by a synergistic effect of gradient thermal annealing (GTA) and anti-solvent treatment.^[164] Such high-quality CsPbI_2Br films realized a sPCE of 15.8% and $\text{rf}V_{\text{OC}} = 1.22$ V.

4.4.2. Ionic Incorporation

Impurity doping by incorporating ions into the host lattice has been extensively explored to modulate CsPbI_2Br film performance, in which the A, B, and X sites have all been substituted.

A-site incorporation: Nam et al. added K^+ into the CsPbI_2Br , resulting in larger crystallites and improved electron extraction.^[53] Planar cells showed an average improvement in reverse scan PCE from 8.2% for CsPbI_2Br to 9.1% for $\text{Cs}_{0.925}\text{K}_{0.075}\text{PbI}_2\text{Br}$, and a best sPCE of 9.2% and $V_{\text{OC}} = 1.18$ V. Moreover, the device containing K^+ shows extended operational lifetime in 20% RH air. Very recently, Gao et al. demonstrated that rubidium (Rb) incorporation in the CsPbI_2Br active layer could enhance both stability and solar cell efficiency. Using Nb_2O_5 as ETL and carbon contact (no HTL), a sPCE of 11.9% and $\text{rf}V_{\text{OC}}$ of 1.21 V were reported.^[165]

B-site incorporation: Lau et al. incorporated Sr as a substituent for Pb.^[166] The surface of the $\text{CsPb}_{1-x}\text{Sr}_x\text{I}_2\text{Br}$ film was enriched with Sr, providing a passivating effect. At the optimal concentration ($x = 0.02$), the PSC (with P3HT as the HTM) achieved a sPCE of 10.8% and V_{OC} of 1.06 V. Yang

et al. added Ge to substitute for Pb and found that this stabilized the cubic phase under high humidity (in the absence of Ge, the HaP changed to the yellow phase while with 20% Ge, there was no visible change after 120 h). Cells ($\text{SnO}_2/\text{HaP}/\text{P3HT/spiro}$) gave an rfPCE of 8.9% and $\text{rf}V_{\text{OC}}$ of 1.23 V (a higher V_{OC} was found for 30% Ge but with a drop in efficiency). The stability in humid air was also much better than the cells without Ge.^[167] Bai et al. added Mn ions and found, mainly from the expansion of the lattice, that the Mn ions lie in the interstices of the CsPbI_2Br lattice structure rather than substituting for Pb during the film-growth process.^[168] Furthermore, the excess Mn^{2+} ions chemisorbed at the grain boundary surfaces provide effective passivation: this resulted in enhanced hole extraction efficiency through decreased recombination loss and advantages in terms of suppressed nucleation and decreased deposition rate, leading to improved microcrystalline thin films (shown in Figure 8a). As a result, the optimized CsPbBrI_2 PSC achieved a sPCE of 13.4% and V_{OC} of 1.17 V. Xiang et al. incorporated Eu into the CsPbI_2Br inorganic perovskite lattice.^[169] With the optimization of the doping concentration of Eu (ca. 5%), they obtained reduced non-radiative recombination, a sPCE of 13.3% and high $V_{\text{OC}} = 1.27$ V.

X-site incorporation: Fu et al. substituted F into the X-site of CsPbBrI_2 with the intention of increasing the tolerance factor through the presence of the small F atom.^[170] Some δ -phase was formed with the dominant α -phase, which was suggested to form a heterojunction between the two phases to enhance charge separation (it was not clear how the two phases were distributed). $\text{CsPbBrI}_{1.78}\text{F}_{0.22}$ PSC displayed a PCE (not specified what type and there was no mention of hysteresis) up to 10.3%, $V_{\text{OC}} = 1.01$ V and structural stability against moisture.

4.4.3. Low-Temperature Preparation

CsPbX_3 generally is prepared at high-temperature (around 300°C is commonly used), which may restrict its application in multilayer or flexible solar cells.^[171] Wang et al. added HI (to form HPbI_{3+x} , as had been used by Eperon et al. to stabilize $\alpha\text{-CsPbI}_3$ at low temperature^[16]) instead of PbI_2 in the one-step preparation at an optimum annealing temperature of 130°C.^[172] The resulting CsPbI_2Br films demonstrated phase stability in air (<20% RH) for a month and thermal stability at 100°C for more than a week. Planar CsPbI_2Br PSCs exhibited a rfPCE of 9.3% and $\text{rf}V_{\text{OC}} = 1.08$ V. By DMSO coordination, Rao et al. deposited CsPbI_2Br at room temperature by using only DMSO as a solvent together with exposing the resulting film to DMSO vapor at room temperature which induced crystallization as well as uniform and void-free films (Figure 8b).^[173] Annealing at 120°C resulted in a further improvement, with cells (inverted, $\text{NiO}/\text{HaP}/\text{bathocuproine}$) giving a PCE of 10.4% and V_{OC} of 1.05 V (scanning direction was not defined). Yin et al. reported an approach for depositing high-quality CsPbI_2Br films via the Lewis base adducts $\text{PbI}_2(\text{DMSO})$ and $\text{PbBr}_2(\text{DMSO})$ as precursors to slow the crystallization of the CsPbI_2Br film.^[174] This process produces CsPbI_2Br films with, after annealing at 200°C, large-scale crystalline grains, flat surfaces,

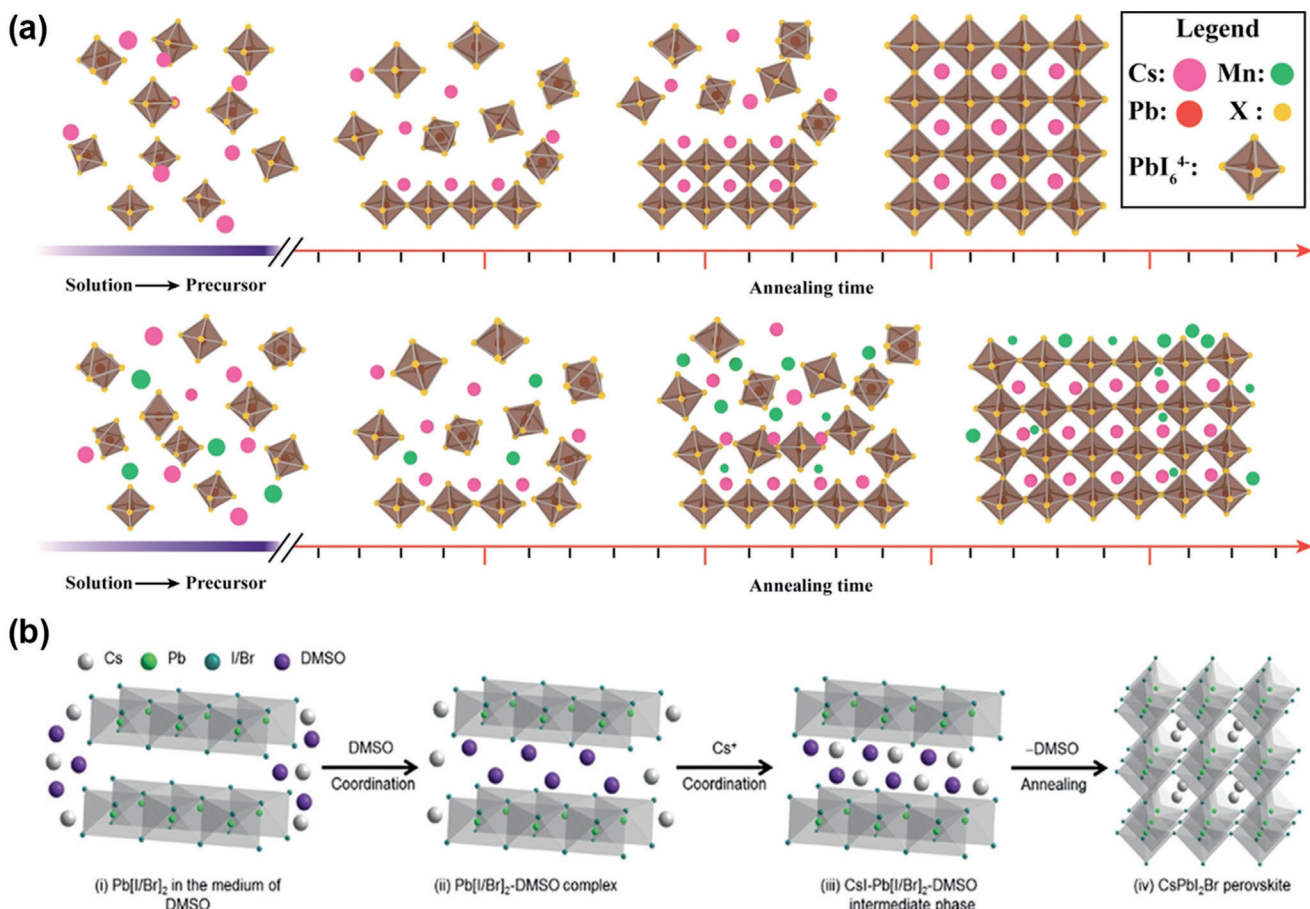


Figure 8. a) Schematic diagram for MnCl₂-driven crystalline grain growth with surface passivation. Reproduced with permission.^[168] Copyright 2018, American Chemical Society Publications. b) Evolution mechanism of the DMSO-induced room-temperature formation of cubic CsPbI₂Br. Reproduced with permission.^[173] Copyright 2018, Wiley-VCH Publications.

low defect densities, and long carrier lifetimes, and the related CsPbI₂Br PSCs exhibited a SPCE of 14.7% and 1.12 V V_{OC} . More interestingly, using this technique, a PCE of 13.5% and 1.18 V V_{OC} were achieved at low annealing temperature (120°C), and enables fabrication of flexible PSCs with PCE of 11.7%.^[175] Zai et al. used DMSO/DMF solvent mixtures at 100°C (using SnO₂ as ETL and PTAA as the HTL) to obtain a SPCE of 14.3% with 1.16 V V_{OC} .^[176]

4.4.4. Interface Engineering

Despite the rapid progress, the PCE achieved to date for the CsPbI₂Br solar cells is still too low, leaving considerable room for further improvement.^[177,178] For a band gap of 1.9 eV, the maximum voltage that can be theoretically extracted from non-concentrated standard sunlight is 1.589 V;^[179] we are still a few hundred mV below this. Non-radiative recombination, mismatched energy levels between HaP and (selective) charge extraction layers, poor intrinsic photoluminescence (PL) quantum efficiency and shorting (which is more likely where the morphology of the HaP layer is poor) can all contribute to the present losses.^[180] Non-radiative recombination can be influenced by the perovskite interfaces with other cell components in several ways: 1) by

recombination at interface states (from the HaP, from the other component or due to interaction between both phases; 2) by modifying the rate of charge extraction (slower extraction favors more recombination—both radiative and non-radiative); 3) if, for example, the conduction band of the HaP is lower than that of the ETL, this will reduce the rate of electron extraction (similarly if the valence band of the HaP is higher than that of the HTL); 4) the opposite of (3), conduction band of the HaP is higher than that of the ETL, in which case a barrier is formed due to the band mismatch and this is (in a simple picture) reflected as a loss in energy (therefore V_{OC}) equal to the size of the barrier. The term “in a simple picture” refers to the well-known electron affinity rule, which predicts heterojunction band lineups based on the electron affinities of each individual component. This rule is, however, very often incorrect.^[181] This is usually due to interactions between the two phases that introduces an interface dipole, but also many energy values are taken from the literature and the values can vary according to details of the sample preparation or exposure to different environments.

Matching energy levels: It was found that nonradiative recombination was largely governed by the mismatched energy levels between the perovskite and the electron

transporting layer (ETL) or hole transporting layer (HTL).^[182,183] Liu et al. used a ZnO@C₆₀ bilayer as the ETL and NiO as the HTL in an inverted cell which demonstrated high electron extraction efficiency and low leakage loss.^[76] The resulting cell yielded a sPCE of around 12 % and rf V_{OC} = 1.09 V. Yan et al. introduced a SnO₂/ZnO bilayered ETL aimed to achieve low energy loss and large V_{OC} for high-efficiency CsPbI₂Br PSCs (shown in Figure 9a).^[184] The higher lying conduction band minimum of ZnO facilitates desirable cascade energy level alignment between CsPbI₂Br and SnO₂/ZnO bilayered ETL with superior electron extraction capability, resulting in a suppressed interfacial trap-assisted recombination with lower charge recombination rate and greater charge extraction efficiency. The cell reached a sPCE of 14.1 % and 1.23 V. Zeng et al. demonstrated that polythiophene, deposited on the top of CsPbI₂Br and a simple annealing process, can significantly reduce electron–hole recombination within the perovskite to minimize the E_{loss}, which is due to the electronic passivation of surface defect states, leading to significantly reduced energy disorder in polythiophene and enhanced hole-injection into the hole-acceptor.^[185] A sPCE of 9.5 % and rf V_{OC} of approximately 1.28 V was obtained.

Band alignment: In the classical structure, an n⁺p abrupt heterojunction with the depletion region is usually located in the CsPbI₂Br film close to the ETL.^[186] Such a phenomenon entails a tapering off of the amplitude of the electric field near the back side of the device—the region in which drift-driven transport is most urgently needed to extract photocharges generated farthest from the n⁺p abrupt junction.^[187] Hence, although a thick perovskite film is beneficial for increased absorbance, a large recombination loss near/at the interface between the CsPbI₂Br and HTL may reduce the device performance. Zhang et al. carried out band alignment by gradually profiling the interface dimensionality to achieve improved device performance.^[186] Bulk-nanosheet-quantum

dots or 3D-2D-0D dimensionally profiled interfaces introduce an electric field in the rear side of the device to promote carrier extraction, resulting in increased current (shown in Figure 9b). In addition, the interface allows for greater electron and hole quasi-Fermi-level splitting at the maximum power point, resulting in an increased operating voltage. As a result, the best-performing device has a sPCE of 12.4 % with V_{OC} = 1.19 V. In further work, post-treatment of the CsPbI₂Br QDs/film with an organic iodine salt formed an ultrathin iodine-ion-enriched perovskite layer on the top of the perovskite film (Figure 9c).^[188] All these procedures (from Refs. [186, 188] combined) generated a favorable field in the cell resulting in effectively decreased recombination loss and improved hole extraction efficiency. As a result, the best device achieved a sPCE of 14.1 % with V_{OC} = 1.223 V.

Grain boundary optimization: It appears that grain boundaries in the perovskite film can cause charge recombination at their associated charge trap states.^[189] Meanwhile, the grain boundaries may induce shallow states near the valence band edge that will hinder hole diffusion.^[168] Yuan et al. introduced a Pb²⁺ solution post-processing strategy to passivate the deep trap states of CsPbI₂Br film.^[190] The Pb²⁺ ion in the precursor solution effectively combines with the excess halide ions on the perovskite surface to reduce deep trap states arising from Pb vacancies (V_{Pb}) and I interstitials (I_I). As a result, the CsPbI₂Br PSC showed a rfPCE of 11.9 % with rf V_{OC} = 1.26 V and relatively low hysteresis. Zeng et al. successfully achieved stable and efficient CsPbI₂Br PECs with rfPCE of 11.5 % and V_{OC} = 1.17 V by adding Pb(Ac)₂ to the precursor solution.^[191] The, Ac⁻ strongly coordinates with CsPbI₂Br grain boundaries and surfaces to stabilize the α-phase and also make the grain size smaller and the film more uniform. PbO is formed in situ at the grain boundary by decomposing Pb(Ac)₂ by high-temperature annealing, which effectively passivates surface states, reduces interface recombination, and promotes charge transport.

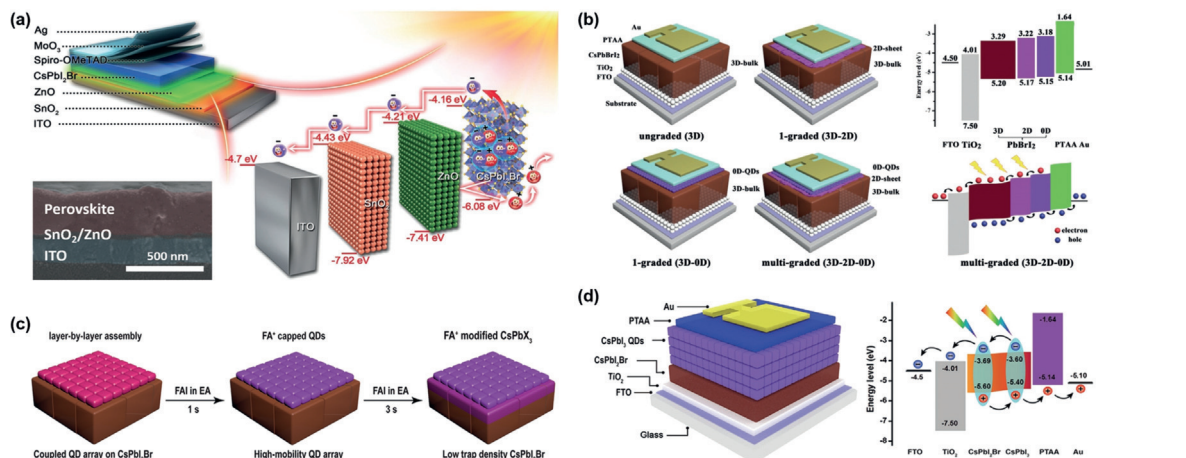


Figure 9. a) Device architecture, energy diagrams, and cross-section SEM image of CsPbI₂Br perovskite film on SnO₂/ZnO. Reproduced with permission.^[184] Copyright 2018, Wiley-VCH Publications. b) Schematic structures of devices without and with a graded interface; energy-level diagram and the carrier-transport mechanism in multi-graded CsPbI₂Br PSCs. Reproduced with permission.^[186] Copyright 2018, Wiley-VCH Publications. c) Schematic diagram of the CsPbI₂Br QDs/film with FAI post-treatment. Reproduced with permission.^[188] Copyright 2018, Wiley-VCH Publications. d) Schematic structure and energy-level diagram of graded E_g CsPbI_{2+x}Br_{1-x} PSC. Reproduced with permission.^[192] Copyright 2018, Elsevier Inc Publications.

4.4.5. Structure Engineering

In this Section, we describe three CsPbI₂Br-based cells with different cell structures than those commonly used. In the first, the concept of parallel stacking of cells with different band gaps is used to broaden the absorption spectrum and increase the short circuit current density (J_{sc} ; although with some loss in V_{OC} from the higher V_{OC} cell). Bian et al. reported an integrated structure based on all-inorganic CsPbI₂Br and CsPbI₃ nanocrystalline films with a graded E_g (shown in Figure 9d) for efficient light harvesting from 300 nm to 700 nm, covering most of the visible solar spectrum.^[192] As the CsPbI₂Br absorbs 300–650 nm light, and the CsPbI₃ QDs film absorbs from 300–700 nm effectively, the combination works like an interlayer-free parallel-connected bilayer film based device.^[193] The broadened external quantum efficiency (EQE) spectrum confirms that enhanced light harvesting is achieved. The electric field induced by the graded E_g is beneficial for improving carrier collection. The combination of extended photoresponse and graded energy structure resulted in a cell (PTAA as the HTL) with sPCE = 14.4% and $V_{OC} = 1.20$ V and very little hysteresis. Wang et al. used a PEACl treatment of the CsPbI₂Br film to increase its hydrophobicity and significantly improve its moisture-resistance without compromising its high solar cell efficiency.^[194] The hydrophobic aromatic group PEA⁺ adsorbs in the edge-on orientation on the CsPbI₂Br surface and the small Cl⁻ is doped into the CsPbI₂Br lattice during the post-annealing, resulting in a contracted lattice. Compared with the reference sample without the PEACl treatment, the cell (PTAA HTM) gave a sPCE of 14.0% and $V_{OC} = 1.22$ V together with much improved moisture resistance. Finally, in a similar incorporation of PEA cation, together with use of HPbX₃ and CsAc, Jiang et al. reported 11.9% PCE and 1.11 V.^[115]

5. Conclusions and Prospects

All-inorganic CsPbX₃ PSCs have shown great promise as an alternative for hybrid PSCs. However, the PCEs of CsPbX₃ PSCs are still significantly lower than the hybrid ones, even taking into account the higher band gaps and therefore lower theoretical efficiencies. The phase instability of α-CsPbI₃ is another problem: although considerable progress has been made in stabilizing this phase or utilizing other black phases, its long-term stability is still in question.

The more stable CsPbI₂Br is a particularly good candidate for higher band gap tandem cell use.^[131] Most of the progress in this material has been made over the past year and we can look forward to more progress in the near future. What is noticeable is that there has been no report (to our knowledge) on partial substitution of Pb by Sn for CsPbI₂Br (although there is one report describing substitution of Pb by Ge,^[167] and one about substitution of Pb by Sn and Ge.^[195]). Since there are many studies on mixed Pb-Sn HaPs in general and it appears that there is no stability problem, as occurs for pure Sn HaPs, for the mixed Pb-Sn HaPs as long as the Sn content is not too high, this substitution should serve the dual purpose

of increasing the phase stability of α-CsPbI₂Br (by increasing the Goldschmidt tolerance factor) as well as reducing the band gap below the approximately 1.9 eV of CsPbI₂Br. We would be surprised if this was still not reported in 2019.

Still with substitution of the Pb, and returning to all the CsPbX₃ family discussed herein, it seems that almost anything added either to substitute the Pb (whether or not the substitution actually occurs) is beneficial for the resulting PV cells. It is more likely that only “successful” experiments (i.e., showing improvement in cell performance) were reported. If so, this is unfortunate since “failures” (according to the same criterion) may be instructive, particularly if studied enough to understand why the “failure” occurred. Probably such “failures” are less likely to be accepted for publication; acknowledging that there may already be more than enough relevant journals, one extra one dedicated to such “failures” may contribute much to scientific progress.

Another fact that stands out is the consistently high values of V_{OC} obtained for the nanocrystalline CsPbI₃ cells, where, out of the four reports using CsPbI₃ nanocrystals, the lowest V_{OC} was 1.18 V and the others were over 1.2 V with the highest being 1.28 V. There were differences in the cell HTLs, but all used the common TiO₂ as ETL; therefore it is unlikely that the cause of the high V_{OC} is connected with the specific cell structures. Considering the importance of V_{OC} if the cells are to be used as top cells in tandems, an understanding of why the nanocrystalline cells give such high (and uniformly high) values of V_{OC} seems essential to obtain the further improvement in V_{OC} .

There is still a lack of understanding in the HaP cell field as to how important the non-HaP cell components are (e.g., matching of energy levels between HaPs and the selective contacts to reduce energy losses often does not follow what is expected from known energy levels, mostly based on the measured levels of the individual materials). However, there is still much room to investigate the effect of cell structure and energetics (of individual components) on the inorganic HaP cell performance, particularly the V_{OC} . Ideally investigations into total cell energy structure should include interface measurements, for example, measuring how the levels of different components change when a second phase is gradually deposited on the first.

Finally (and this is true for both all-inorganic and hybrid cells), we still do not know why the voltage efficiency of the bromide cells are so much poorer than the iodide ones. Is this may be related to the greater Urbach energies intrinsic to the bromide HaPs or is there some other specific reason for this difference?

Acknowledgements

This work was funded by the National Key Research and Development Program of China MOST (2017YFA0204800), National Natural Science Foundation of China (61704099/91733301), DNL Cooperation Fund CAS (DNL180311), Key Laboratory for Magnetism and Magnetic Materials of the Ministry of Education (LZUMMM2019001/LZUMMM2019005), CAS Natural Science Foundation of

Shaanxi Province (2018JQ6072), and the 111 Project (B14041).

Conflict of interest

The authors declare no conflict of interest.

How to cite: *Angew. Chem. Int. Ed.* **2019**, *58*, 15596–15618
Angew. Chem. **2019**, *131*, 15742–15765

- [1] Z. Liang, M. Su, H. Wang, Y. Gong, F. Xie, L. Gong, H. Meng, P. Liu, H. Chen, W. Xie, J. Chen, *ACS Appl. Mater. Interfaces* **2015**, *7*, 5830–5836.
- [2] M. L. Tsai, W. C. Tu, L. Tang, T. C. Wei, W. R. Wei, S. P. Lau, L. J. Chen, J. H. He, *Nano Lett.* **2016**, *16*, 309–313.
- [3] C.-H. Chang, Y.-L. Lee, *Appl. Phys. Lett.* **2007**, *91*, 053503.
- [4] J.-H. Yum, E. Baranoff, F. Kessler, T. Moehl, S. Ahmad, T. Bessho, A. Marchioro, E. Ghadiri, J.-E. Moser, C. Yi, M. K. Nazeeruddin, M. Grätzel, *Nat. Commun.* **2012**, *3*, 631.
- [5] Z.-G. Zhang, B. Qi, Z. Jin, D. Chi, Z. Qi, Y. Li, J. Wang, *Energy Environ. Sci.* **2014**, *7*, 1966–1973.
- [6] Z. Jin, A. Wang, Q. Zhou, Y. Wang, J. Wang, *Sci. Rep.* **2016**, *6*, 37106.
- [7] X. Zhang, Q. Wang, Z. Jin, Y. Chen, H. Liu, J. Wang, Y. Li, S. Liu, *Adv. Mater. Interfaces* **2018**, *5*, 1701117.
- [8] J. Jiang, Q. Wang, Z. Jin, X. Zhang, J. Lei, H. Bin, Z.-G. Zhang, Y. Li, S. Liu, *Adv. Energy Mater.* **2018**, *8*, 1701757.
- [9] A. Kojima, K. Teshima, Y. Shirai, T. Miyasaka, *J. Am. Chem. Soc.* **2009**, *131*, 6050–6051.
- [10] NREL, *Best Research-Cell Efficiencies* **2019**, <https://www.nrel.gov/pv/assets/pdfs/pv-efficiency-chart.20181214.pdf>.
- [11] J. Liang, Z. Liu, L. Qiu, Z. Hawash, L. Meng, Z. Wu, Y. Jiang, L. K. Ono, Y. Qi, *Adv. Energy Mater.* **2018**, *8*, 1800504.
- [12] C. Yi, J. Luo, S. Meloni, A. Boziki, N. Ashari-Astani, C. Grätzel, S. M. Zakeeruddin, U. Röhlisberger, M. Grätzel, *Energy Environ. Sci.* **2016**, *9*, 656–662.
- [13] Q. Wang, X. Zhang, Z. Jin, J. Zhang, Z. Gao, Y. Li, S. Liu, *ACS Energy Lett.* **2017**, *2*, 1479–1486.
- [14] Q. Zeng, X. Zhang, C. Liu, T. Feng, Z. Chen, W. Zhang, W. Zheng, H. Zhang, B. Yang, *Sol. RRL* **2019**, *3*, 1800239.
- [15] M. Kulbak, D. Cahen, G. Hodes, *J. Phys. Chem. Lett.* **2015**, *6*, 2452–2456.
- [16] G. E. Eperon, G. M. Paternò, R. J. Sutton, A. Zampetti, A. A. Haghhighirad, F. Cacialli, H. J. Snaith, *J. Mater. Chem. A* **2015**, *3*, 19688–19695.
- [17] Y. Wang, T. Zhang, M. Kan, Y. Zhao, *J. Am. Chem. Soc.* **2018**, *140*, 12345–12348.
- [18] W. Ke, I. Spanopoulos, C. C. Stoumpos, M. G. Kanatzidis, *Nat. Commun.* **2018**, *9*, 4785.
- [19] M. Abdi-Jalebi, Z. Andajai-Garmaroudi, S. Cacovich, C. Stavrakas, B. Philippe, J. M. Richter, M. Alsari, E. P. Booker, E. M. Hutter, A. J. Pearson, S. Lilliu, T. J. Savenije, H. Rensmo, G. Divitini, C. Ducati, R. H. Friend, S. D. Stranks, *Nature* **2018**, *555*, 497.
- [20] J.-W. Lee, D.-H. Kim, H.-S. Kim, S.-W. Seo, S. M. Cho, N.-G. Park, *Adv. Energy Mater.* **2015**, *5*, 1501310.
- [21] M. Saliba, T. Matsui, J.-Y. Seo, K. Domanski, J.-P. Correa-Baena, M. K. Nazeeruddin, S. M. Zakeeruddin, W. Tress, A. Abate, A. Hagfeldt, M. Grätzel, *Energy Environ. Sci.* **2016**, *9*, 1989–1997.
- [22] X. Zhang, Q. Wang, Z. Jin, J. Zhang, S. Liu, *Nanoscale* **2017**, *9*, 6278–6285.
- [23] A. Marronnier, G. Roma, S. Boyer-Richard, L. Pedesseau, J.-M. Jancu, Y. Bonnassieux, C. Katan, C. C. Stoumpos, M. G. Kanatzidis, J. Even, *ACS Nano* **2018**, *12*, 3477–3486.
- [24] I. Lignos, V. Morad, Y. Shynkarenko, C. Bernasconi, R. M. Maceiczyk, L. Protesescu, F. Bertolotti, S. Kumar, S. T. Ochsenbein, N. Masciocchi, A. Guagliardi, C.-J. Shih, M. I. Bodnarchuk, A. J. deMello, M. V. Kovalenko, *ACS Nano* **2018**, *12*, 5504–5517.
- [25] S. Dastidar, C. J. Hawley, A. D. Dillon, A. D. Gutierrez-Perez, J. E. Spanier, A. T. Fafarman, *J. Phys. Chem. Lett.* **2017**, *8*, 1278–1282.
- [26] C. C. Stoumpos, C. D. Malliakas, M. G. Kanatzidis, *Inorg. Chem.* **2013**, *52*, 9019–9038.
- [27] T. Burwig, W. Franzel, P. Pistor, *J. Phys. Chem. Lett.* **2018**, *9*, 4808–4813.
- [28] V. M. Goldschmidt, *Naturwissenschaften* **1926**, *14*, 477–485.
- [29] Z. Li, M. Yang, J.-S. Park, S.-H. Wei, J. J. Berry, K. Zhu, *Chem. Mater.* **2016**, *28*, 284–292.
- [30] Y. Fu, M. T. Rea, J. Chen, D. J. Morrow, M. P. Hautzinger, Y. Zhao, D. Pan, L. H. Manger, J. C. Wright, R. H. Goldsmith, S. Jin, *Chem. Mater.* **2017**, *29*, 8385–8394.
- [31] X. Liu, D. Yu, X. Song, H. Zeng, *Small* **2018**, *14*, 1801460.
- [32] R. X. Yang, J. M. Skelton, E. L. da Silva, J. M. Frost, A. Walsh, *J. Phys. Chem. Lett.* **2017**, *8*, 4720–4726.
- [33] C. C. Stoumpos, C. D. Malliakas, J. A. Peters, Z. Liu, M. Sebastian, J. Im, T. C. Chasapis, A. C. Wibowo, D. Y. Chung, A. J. Freeman, B. W. Wessels, M. G. Kanatzidis, *Cryst. Growth Des.* **2013**, *13*, 2722–2727.
- [34] Y. Guo, Q. Wang, W. A. Saidi, *J. Phys. Chem. C* **2017**, *121*, 1715–1722.
- [35] V. K. Ravi, G. B. Markad, A. Nag, *ACS Energy Lett.* **2016**, *1*, 665–671.
- [36] L. Protesescu, S. Yakunin, M. I. Bodnarchuk, F. Krieg, R. Caputo, C. H. Hendon, R. X. Yang, A. Walsh, M. V. Kovalenko, *Nano Lett.* **2015**, *15*, 3692–3696.
- [37] X. Li, Y. Wu, S. Zhang, B. Cai, Y. Gu, J. Song, H. Zeng, *Adv. Funct. Mater.* **2016**, *26*, 2435–2445.
- [38] A. Filippetti, A. Mattoni, *Phys. Rev. B* **2014**, *89*, 125203.
- [39] X. Li, F. Cao, D. Yu, J. Chen, Z. Sun, Y. Shen, Y. Zhu, L. Wang, Y. Wei, Y. Wu, H. Zeng, *Small* **2017**, *13*, 1603996.
- [40] R. A. Jishi, O. B. Ta, A. A. Sharif, *J. Phys. Chem. C* **2014**, *118*, 28344–28349.
- [41] Z. Yang, A. Surrente, K. Galkowski, A. Miyata, O. Portugall, R. J. Sutton, A. A. Haghhighirad, H. J. Snaith, D. K. Maude, P. Plochocka, R. J. Nicholas, *ACS Energy Lett.* **2017**, *2*, 1621–1627.
- [42] K. Galkowski, A. Mitioglu, A. Miyata, P. Plochocka, O. Portugall, G. E. Eperon, J. T.-W. Wang, T. Stergiopoulos, S. D. Stranks, H. J. Snaith, R. J. Nicholas, *Energy Environ. Sci.* **2016**, *9*, 962–970.
- [43] S. Poncé, M. Schlipf, F. Giustino, *ACS Energy Lett.* **2019**, *4*, 456–463.
- [44] D. A. Egger, A. Bera, D. Cahen, G. Hodes, T. Kirchartz, L. Kronik, R. Lovrincic, A. M. Rappe, D. R. Reichman, O. Yaffe, *Adv. Mater.* **2018**, *30*, 1800691.
- [45] Y. Huang, W.-J. Yin, Y. He, *J. Phys. Chem. C* **2018**, *122*, 1345–1350.
- [46] C. C. Stoumpos, M. G. Kanatzidis, *Acc. Chem. Res.* **2015**, *48*, 2791–2802.
- [47] K. T. Butler, *J. Mater. Chem. C* **2018**, *6*, 12045–12051.
- [48] J. Chen, N.-G. Park, *Adv. Mater.* **2018**, <https://doi.org/10.1002/adma.201803019>.
- [49] E. M. Hutter, R. J. Sutton, S. Chandrashekhar, M. Abdi-Jalebi, S. D. Stranks, H. J. Snaith, T. J. Savenije, *ACS Energy Lett.* **2017**, *2*, 1901–1908.
- [50] S. Dastidar, S. Li, S. Y. Smolin, J. B. Baxter, A. T. Fafarman, *ACS Energy Lett.* **2017**, *2*, 2239–2244.
- [51] C. L. Kennedy, A. H. Hill, E. S. Massaro, E. M. Grumstrup, *ACS Energy Lett.* **2017**, *2*, 1501–1506.

- [52] H. Zhu, M. T. Trinh, J. Wang, Y. Fu, P. P. Joshi, K. Miyata, S. Jin, X.-Y. Zhu, *Adv. Mater.* **2017**, *29*, 1603072.
- [53] J. K. Nam, S. U. Chai, W. Cha, Y. J. Choi, W. Kim, M. S. Jung, J. Kwon, D. Kim, J. H. Park, *Nano Lett.* **2017**, *17*, 2028–2033.
- [54] J. Song, Q. Cui, J. Li, J. Xu, Y. Wang, L. Xu, J. Xue, Y. Dong, T. Tian, H. Sun, H. Zeng, *Adv. Opt. Mater.* **2017**, *5*, 1700157.
- [55] M. Kulbak, I. Levine, E. Barak-Kulbak, S. Gupta, A. Zohar, I. Balberg, G. Hodes, D. Cahen, *Adv. Energy Mater.* **2018**, *8*, 1800398.
- [56] G. A. Elbaz, D. B. Straus, O. E. Semonin, T. D. Hull, D. W. Paley, P. Kim, J. S. Owen, C. R. Kagan, X. Roy, *Nano Lett.* **2017**, *17*, 1727–1732.
- [57] A. S. Thind, G. Luo, J. A. Hachtel, M. V. Morrell, S. B. Cho, A. Y. Borisevich, J.-C. Idrobo, Y. Xing, R. Mishra, *Adv. Mater.* **2019**, *31*, 1805047.
- [58] J. Kang, L.-W. Wang, *J. Phys. Chem. Lett.* **2017**, *8*, 489–493.
- [59] E. M. Hutter, T. J. Savenije, *ACS Energy Lett.* **2018**, *3*, 2068–2069.
- [60] M. Kulbak, S. Gupta, N. Kedem, I. Levine, T. Bendikov, G. Hodes, D. Cahen, *J. Phys. Chem. Lett.* **2016**, *7*, 167–172.
- [61] S. Mariotti, O. S. Hutter, L. J. Phillips, P. J. Yates, B. Kundu, K. Durose, *ACS Appl. Mater. Interfaces* **2018**, *10*, 3750–3760.
- [62] Y. Li, Y. Wang, T. Zhang, S. Yoriya, P. Kunrnorkaew, S. Chen, X. Guo, Y. Zhao, *Chem. Commun.* **2018**, *54*, 9809.
- [63] A. F. Akbulatov, S. Y. Luchkin, L. A. Frolova, N. N. Dremova, K. L. Gerasimov, I. S. Zhidkov, D. V. Anokhin, E. Z. Kurmaev, K. J. Stevenson, P. A. Troshin, *J. Phys. Chem. Lett.* **2017**, *8*, 1211–1218.
- [64] C. Xiao, Z. Li, H. Guthrey, J. Moseley, Y. Yang, S. Wozny, H. Moutinho, B. To, J. J. Berry, B. Gorman, Y. Yan, K. Zhu, M. Al-Jassim, *J. Phys. Chem. C* **2015**, *119*, 26904–26911.
- [65] S. Sanchez, N. Christoph, B. Grobety, N. Phung, U. Steiner, M. Saliba, A. Abate, *Adv. Energy Mater.* **2018**, *8*, 1802060.
- [66] E. T. Hoke, D. J. Slotcavage, E. R. Dohner, A. R. Bowring, H. I. Karunadasa, M. D. McGehee, *Chem. Sci.* **2015**, *6*, 613–617.
- [67] W. Zhou, Y. Zhao, X. Zhou, R. Fu, Q. Li, Y. Zhao, K. Liu, D. Yu, Q. Zhao, *J. Phys. Chem. Lett.* **2017**, *8*, 4122–4128.
- [68] W. J. Yin, Y. Yan, S. H. Wei, *J. Phys. Chem. Lett.* **2014**, *5*, 3625–3631.
- [69] D. R. Ceratti, Y. Rakita, L. Cremonesi, R. Tenne, V. Kalchenko, M. Elbaum, D. Oron, M. A. C. Potenza, G. Hodes, D. Cahen, *Adv. Mater.* **2018**, *30*, 1706273.
- [70] W. Nie, J.-C. Blancon, A. J. Neukirch, K. Appavoo, H. Tsai, M. Chhowalla, M. A. Alam, M. Y. Sfeir, C. Katan, J. Even, S. Tretiak, J. J. Crochet, G. Gupta, A. D. Mohite, *Nat. Commun.* **2016**, *7*, 11574.
- [71] D. Ding, H. Li, J. Li, Z. Li, H. Yao, L. Liu, B. B. Tian, C. Su, F. Chen, Y. Shi, *J. Mater. Chem. A* **2019**, *7*, 540–548.
- [72] M. L. Petrus, J. Schlipf, C. Li, T. P. Gujar, N. Giesbrecht, P. Müller-Buschbaum, M. Thelakkat, T. Bein, S. Hüttner, P. Docampo, *Adv. Energy Mater.* **2017**, *7*, 1700264.
- [73] P. Mao, Q. Zhou, Z. Jin, H. Li, J. Wang, *ACS Appl. Mater. Interfaces* **2016**, *8*, 23837–23843.
- [74] Q. A. Akkerman, M. Gandini, F. Di Stasio, P. Rastogi, F. Palazon, G. Bertoni, J. M. Ball, M. Prato, A. Petrozza, L. Manna, *Nat. Energy* **2016**, *2*, 16194.
- [75] D. Bai, H. Bian, Z. Jin, H. Wang, L. Meng, Q. Wang, S. Liu, *Nano Energy* **2018**, *52*, 408–415.
- [76] C. Liu, W. Li, C. Zhang, Y. Ma, J. Fan, Y. Mai, *J. Am. Chem. Soc.* **2018**, *140*, 3825–3828.
- [77] J. Duan, Y. Zhao, B. He, Q. Tang, *Angew. Chem. Int. Ed.* **2018**, *57*, 3787–3791; *Angew. Chem.* **2018**, *130*, 3849–3853.
- [78] Y. Li, J. Duan, H. Yuan, Y. Zhao, B. He, Q. Tang, *Sol. RRL* **2018**, *2*, 1800164.
- [79] P. Wang, X. Zhang, Y. Zhou, Q. Jiang, Q. Ye, Z. Chu, X. Li, X. Yang, Z. Yin, J. You, *Nat. Commun.* **2018**, *9*, 2225.
- [80] D. Prochowicz, M. M. Tavakoli, A. Solanki, T. W. Goh, K. Pandey, T. C. Sum, M. Saliba, P. Yadav, *J. Mater. Chem. A* **2018**, *6*, 14307–14314.
- [81] Y. Rakita, N. Kedem, S. Gupta, A. Sadhanala, V. Kalchenko, M. L. Böhm, M. Kulbak, R. H. Friend, D. Cahen, G. Hodes, *Crust. Growth Des.* **2016**, *16*, 5717–5725.
- [82] X. Zhang, Z. Jin, J. Zhang, D. Bai, H. Bian, K. Wang, J. Sun, Q. Wang, S. Liu, *ACS Appl. Mater. Interfaces* **2018**, *10*, 7145–7154.
- [83] A. J. Ramadan, L. A. Rochford, S. Fearn, H. J. Snaith, *J. Phys. Chem. Lett.* **2017**, *8*, 4172–4176.
- [84] B. Yu, H. Zhang, J. Wu, H. Li, Y. Li, J. Shi, H. Wu, D. Li, Y. Luo, Q. Meng, *J. Mater. Chem. A* **2018**, *6*, 19810–19816.
- [85] A. Swarnkar, A. R. Marshall, E. M. Sanehira, B. D. Chernomordik, D. T. Moore, J. A. Christians, T. Chakrabarti, J. M. Luther, *Science* **2016**, *354*, 92–95.
- [86] Q. Wang, Z. Jin, D. Chen, D. Bai, H. Bian, J. Sun, G. Zhu, G. Wang, S. Liu, *Adv. Energy Mater.* **2018**, *8*, 1800007.
- [87] J. Li, L. Xu, T. Wang, J. Song, J. Chen, J. Xue, Y. Dong, B. Cai, Q. Shan, B. Han, H. Zeng, *Adv. Mater.* **2017**, *29*, 201603885.
- [88] X. Li, D. Yu, F. Cao, Y. Gu, Y. Wei, Y. Wu, J. Song, H. Zeng, *Adv. Funct. Mater.* **2016**, *26*, 5903–5912.
- [89] J. Lei, F. Gao, H. Wang, J. Li, J. Jiang, X. Wu, R. Gao, Z. Yang, S. Liu, *Sol. Energy Mater. Sol. Cells* **2018**, *187*, 1–8.
- [90] C. K. Möller, *Nature* **1958**, *182*, 1436.
- [91] H. Choi, J. Jeong, H. B. Kim, S. Kim, B. Walker, G. H. Kim, Y. K. Jin, *Nano Energy* **2014**, *7*, 80–85.
- [92] P. Luo, W. Xia, S. Zhou, L. Sun, J. Cheng, C. Xu, Y. Lu, *J. Phys. Chem. Lett.* **2016**, *7*, 3603–3608.
- [93] T. S. Ripolles, K. Nishinaka, Y. Ogomi, Y. Miyata, S. Hayase, *Sol. Energy Mater. Sol. Cells* **2016**, *144*, 532–536.
- [94] K. Yonezawa, K. Yamamoto, M. Shahiduzzaman, Y. Furumoto, K. Hamada, T. S. Ripolles, M. Karakawa, T. Kuwabara, K. Takahashi, S. Hayase, T. Taima, *Jpn. J. Appl. Phys.* **2017**, *56*, 04CS11.
- [95] L. A. Frolova, D. V. Anokhin, A. A. Piryazev, S. Y. Luchkin, N. N. Dremova, K. J. Stevenson, P. A. Troshin, *J. Phys. Chem. Lett.* **2017**, *8*, 67–72.
- [96] S. Xiang, Z. Fu, W. Li, Y. Wei, J. Liu, H. Liu, L. Zhu, R. Zhang, H. Chen, *ACS Energy Lett.* **2018**, *3*, 1824–1831.
- [97] A. Swarnkar, W. J. Mir, A. Nag, *ACS Energy Lett.* **2018**, *3*, 286–289.
- [98] R. J. Sutton, M. R. Filip, A. A. Haghhighirad, N. Sakai, B. Wenger, F. Giustino, H. J. Snaith, *ACS Energy Lett.* **2018**, *3*, 1787–1794.
- [99] B. Zhao, S. Jin, S. Huang, N. Liu, J. Y. Ma, D. J. Xue, Q. Han, J. Ding, Q. O. Ge, Y. Feng, J. S. Hu, *J. Am. Chem. Soc.* **2018**, *140*, 11716–11725.
- [100] J.-K. Sun, S. Huang, X.-Z. Liu, Q. Xu, Q.-H. Zhang, W.-J. Jiang, D.-J. Xue, J.-C. Xu, J.-Y. Ma, J. Ding, Q.-Q. Ge, L. Gu, X.-H. Fang, H.-Z. Zhong, J.-S. Hu, L.-J. Wan, *J. Am. Chem. Soc.* **2018**, *140*, 11705–11715.
- [101] K. Wang, Z. Jin, L. Liang, H. Bian, D. Bai, H. Wang, J. Zhang, Q. Wang, S. Liu, *Nat. Commun.* **2018**, *9*, 4544.
- [102] K. Wang, Z. Jin, L. Liang, H. Bian, H. Wang, J. Feng, Q. Wang, S. Liu, *Nano Energy* **2019**, *58*, 175–182.
- [103] L. Liang, M. Liu, Z. Jin, Q. Wang, H. Wang, H. Bian, F. Shi, S. Liu, *Nano Lett.* **2019**, <https://doi.org/10.1021/acs.nanolett.8b04842>.
- [104] H. Bian, Q. Wang, S. Yang, C. Yan, H. Wang, L. Liang, Z. Jin, G. Wang, S. Liu, *J. Mater. Chem. A* **2019**, *7*, 5740–5747.
- [105] M. J. Mayo, A. Suresh, W. D. Porter, *Rev. Adv. Mater. Sci.* **2003**, *5*, 100–109.
- [106] K. Chen, X. Deng, G. Dodekatos, H. Tüysüz, *J. Am. Chem. Soc.* **2017**, *139*, 12267–12273.
- [107] F. Liu, Y. Zhang, C. Ding, T. Toyoda, Y. Ogomi, T. S. Ripolles, S. Hayase, T. Minemoto, K. Yoshino, S. Dai, Q. Shen, *J. Phys. Chem. Lett.* **2018**, *9*, 294–297.

- [108] E. M. Sanehira, A. R. Marshall, J. A. Christians, S. P. Harvey, P. N. Ciesielski, L. M. Wheeler, P. Schulz, L. Y. Lin, M. C. Beard, J. M. Luther, *Sci. Adv.* **2017**, *3*, eaao4204.
- [109] L. M. Wheeler, E. M. Sanehira, A. R. Marshall, P. Schulz, M. Suri, N. C. Anderson, J. A. Christians, D. Nordlund, D. Sokaras, T. Kroll, S. P. Harvey, J. J. Berry, L. Y. Lin, J. M. Luther, *J. Am. Chem. Soc.* **2018**, *140*, 10504–10513.
- [110] J. Yuan, X. Ling, D. Yang, F. Li, S. Zhou, J. Shi, Y. Qian, J. Hu, Y. Sun, Y. Yang, X. Gao, S. Duhm, Q. Zhang, W. Ma, *Joule* **2018**, *2*, 2450–2463.
- [111] A. Dutta, S. K. Dutta, S. Das Adhikari, N. Pradhan, *Angew. Chem. Int. Ed.* **2018**, *57*, 9083–9087; *Angew. Chem.* **2018**, *130*, 9221–9225.
- [112] I. C. Smith, E. T. Hoke, D. Solis-Ibarra, M. D. McGehee, H. I. Karunadasa, *Angew. Chem. Int. Ed.* **2014**, *53*, 11232–11235; *Angew. Chem.* **2014**, *126*, 11414–11417.
- [113] J.-F. Liao, H.-S. Rao, B.-X. Chen, D.-B. Kuang, C.-Y. Su, *J. Mater. Chem. A* **2017**, *5*, 2066–2072.
- [114] F. Li, Y. Pei, F. Xiao, T. Zeng, Z. Yang, J. Xu, J. Sun, B. Peng, M. Liu, *Nanoscale* **2018**, *10*, 6318–6322.
- [115] Y. Jiang, J. Yuan, Y. Ni, J. Yang, Y. Wang, T. Jiu, M. Yuan, J. Chen, *Joule* **2018**, *2*, 1356–1368.
- [116] T. Zhang, M. I. Dar, G. Li, F. Xu, N. Guo, M. Grätzel, Y. Zhao, *Sci. Adv.* **2017**, *3*, e1700841.
- [117] B. Li, Y. Zhang, L. Fu, T. Yu, S. Zhou, L. Zhang, L. Yin, *Nat. Commun.* **2018**, *9*, 1076.
- [118] B. Jeong, H. Han, Y. J. Choi, S. H. Cho, E. H. Kim, S. W. Lee, J. S. Kim, C. Park, D. Kim, C. Park, *Adv. Funct. Mater.* **2018**, *28*, 1706401.
- [119] Q. Wang, X. Zheng, Y. Deng, J. Zhao, Z. Chen, J. Huang, *Joule* **2017**, *1*, 371–382.
- [120] Y. Wang, T. Zhang, M. Kan, Y. Li, T. Wang, Y. Zhao, *Joule* **2018**, *2*, 2065–2075.
- [121] X. Ding, H. Chen, Y. Wu, S. Ma, S. Dai, S. Yang, J. Zhu, *J. Mater. Chem. A* **2018**, *6*, 18258–18266.
- [122] F. Liu, C. Ding, Y. Zhang, T. S. Ropelles, T. Kamisaka, T. Toyoda, S. Hayase, T. Minemoto, K. Yoshino, S. Dai, M. Yanagida, H. Noguchi, Q. Shen, *J. Am. Chem. Soc.* **2017**, *139*, 16708–16719.
- [123] Y. Hu, F. Bai, X. Liu, Q. Ji, X. Miao, T. Qiu, S. Zhang, *ACS Energy Lett.* **2017**, *2*, 2219–2227.
- [124] Y. Hu, S. Zhang, T. Shu, T. Qiu, F. Bai, W. Ruan, F. Xu, *J. Mater. Chem. A* **2018**, *6*, 20365–20373.
- [125] C. F. J. Lau, X. Deng, J. Zheng, J. Kim, Z. Zhang, M. Zhang, J. Bing, B. Wilkinson, L. Hu, R. Patterson, S. Huang, A. Ho-Baillie, *J. Mater. Chem. A* **2018**, *6*, 5580–5586.
- [126] S. Xiang, W. Li, Y. Wei, J. Liu, H. Liu, L. Zhu, H. Chen, *Nanoscale* **2018**, *10*, 9996–10004.
- [127] A. K. Jena, A. Kulkarni, Y. Sanehira, M. Ikegami, T. Miyasaka, *Chem. Mater.* **2018**, *30*, 6668–6674.
- [128] Q. A. Akkerman, D. Meggiolaro, Z. Dang, F. De Angelis, L. Manna, *ACS Energy Lett.* **2017**, *2*, 2183–2186.
- [129] X. Chang, W. Li, L. Zhu, H. Liu, H. Geng, S. Xiang, J. Liu, H. Chen, *ACS Appl. Mater. Interfaces* **2016**, *8*, 33649–33655.
- [130] X. Liu, X. Tan, Z. Liu, H. Ye, B. Sun, T. Shi, Z. Tang, G. Liao, *Nano Energy* **2019**, *56*, 184–195.
- [131] C. J. Yang, P. Fiala, Q. Jeangros, C. Ballif, *Joule* **2018**, *2*, 1421–1436.
- [132] J. B. Hoffman, G. Zaiats, I. Wappes, P. V. Kamat, *Chem. Mater.* **2017**, *29*, 9767–9774.
- [133] I. Poli, J. Baker, J. McGettrick, F. De Rossi, S. Eslava, T. M. Watson, P. J. Cameron, *J. Mater. Chem. A* **2018**, *6*, 18677–18686.
- [134] H. Yuan, Y. Zhao, J. Duan, Y. Wang, X. Yang, Q. Tang, *J. Mater. Chem. A* **2018**, *6*, 24324–24329.
- [135] J. Liang, C. Wang, Y. Wang, Z. Xu, Z. Lu, Y. Ma, H. Zhu, Y. Hu, C. Xiao, X. Yi, G. Zhu, H. Lv, L. Ma, T. Chen, Z. Tie, Z. Jin, J. Liu, *J. Am. Chem. Soc.* **2016**, *138*, 15829–15832.
- [136] B. Li, Y. Zhang, L. Zhang, L. Yin, *J. Power Sources* **2017**, *360*, 11–20.
- [137] J. Duan, T. Hu, Y. Zhao, B. He, Q. Tang, *Angew. Chem. Int. Ed.* **2018**, *57*, 5746–5749; *Angew. Chem.* **2018**, *130*, 5848–5851.
- [138] J. Duan, Y. Zhao, X. Yang, Y. Wang, B. He, Q. Tang, *Adv. Energy Mater.* **2018**, *8*, 1802346.
- [139] S. Y. Luchkin, A. F. Akbulatov, L. A. Frolova, S. A. Tsarev, P. A. Troshin, K. J. Stevenson, *Sol. Energy Mater. Sol. Cells* **2017**, *171*, 205–212.
- [140] H. Li, G. Tong, T. Chen, H. Zhu, G. Li, Y. Chang, L. Wang, Y. Jiang, *J. Mater. Chem. A* **2018**, *6*, 14255–14261.
- [141] W. Chen, J. Zhang, G. Xu, R. Xue, Y. Li, Y. Zhou, J. Hou, Y. Li, *Adv. Mater.* **2018**, *30*, 1800855.
- [142] S. Panigrahi, S. Jana, T. Calmeiro, D. Nunes, R. Martins, E. Fortunato, *ACS Nano* **2017**, *11*, 10214–10221.
- [143] B. Yang, M. Wang, X. Hu, T. Zhou, Z. Zang, *Nano Energy* **2019**, *57*, 718–727.
- [144] Q. Zhang, W. Zhu, D. Chen, Z. Zhang, Z. Lin, J. Chang, J. Zhang, C. Zhang, Y. Hao, *ACS Appl. Mater. Interfaces* **2019**, *11*, 2997–3005.
- [145] R. E. Beal, D. J. Slotcavage, T. Leijtens, A. R. Bowring, R. A. Belisle, W. H. Nguyen, G. F. Burkhard, E. T. Hoke, M. D. McGehee, *J. Phys. Chem. Lett.* **2016**, *7*, 746–751.
- [146] W. Li, M. U. Rothmann, A. Liu, Z. Wang, Y. Zhang, A. R. Pascoe, J. Lu, L. Jiang, Y. Chen, F. Huang, Y. Peng, Q. Bao, J. Etheridge, U. Bach, Y.-B. Cheng, *Adv. Energy Mater.* **2017**, *7*, 1700946.
- [147] Q. Ma, S. Huang, X. Wen, M. A. Green, A. W. Y. Ho-Baillie, *Adv. Energy Mater.* **2016**, *6*, 1502202.
- [148] C. F. J. Lau, X. Deng, Q. Ma, J. Zheng, J. S. Yun, M. A. Green, S. Huang, A. W. Y. Ho-Baillie, *ACS Energy Lett.* **2016**, *1*, 573–577.
- [149] C. Liu, W. Li, J. Chen, J. Fan, Y. Mai, R. E. I. Schropp, *Nano Energy* **2017**, *41*, 75–83.
- [150] W. Zhu, Q. Zhang, D. Chen, Z. Zhang, Z. Lin, J. Chang, J. Zhang, C. Zhang, Y. Hao, *Adv. Energy Mater.* **2018**, *8*, 1802080.
- [151] J. Lin, M. Lai, L. Dou, C. S. Kley, H. Chen, F. Peng, J. Sun, D. Lu, S. A. Hawks, C. Xie, F. Cui, A. P. Alivisatos, D. T. Limmer, P. Yang, *Nat. Mater.* **2018**, *17*, 261–267.
- [152] J. Liang, P. Zhao, C. Wang, Y. Wang, Y. Hu, G. Zhu, L. Ma, J. Liu, Z. Jin, *J. Am. Chem. Soc.* **2017**, *139*, 14009–14012.
- [153] N. Li, Z. Zhu, J. Li, A. K. Y. Jen, L. Wang, *Adv. Energy Mater.* **2018**, *8*, 1800525.
- [154] J. S. Niezgoda, B. J. Foley, A. Z. Chen, J. J. Choi, *ACS Energy Lett.* **2017**, *2*, 1043–1049.
- [155] R. J. Sutton, G. E. Eperon, L. Miranda, E. S. Parrott, B. A. Kamino, J. B. Patel, M. T. Hörrantner, M. B. Johnston, A. A. Haghhighirad, D. T. Moore, H. J. Snaith, *Adv. Energy Mater.* **2016**, *6*, 1502458.
- [156] X. Meng, Z. Wang, W. Qian, Z. Zhu, T. Zhang, Y. Bai, C. Hu, S. Xiao, Y. Yang, S. Yang, *J. Phys. Chem. Lett.* **2019**, *10*, 194–199.
- [157] Z. Li, J. Xu, S. Zhou, B. Zhang, X. Liu, S. Dai, J. Yao, *ACS Appl. Mater. Interfaces* **2018**, *10*, 38183–38192.
- [158] Q. Ma, S. Huang, S. Chen, M. Zhang, C. F. J. Lau, M. N. Lockrey, H. K. Mulmudi, Y. Shan, J. Yao, J. Zheng, X. Deng, K. Catchpole, M. A. Green, A. W. Y. Ho-Baillie, *J. Phys. Chem. C* **2017**, *121*, 19642–19649.
- [159] C.-Y. Chen, H.-Y. Lin, K.-M. Chiang, W.-L. Tsai, Y.-C. Huang, C.-S. Tsao, H.-W. Lin, *Adv. Mater.* **2017**, *29*, 1605290.
- [160] J. K. Nam, M. S. Jung, S. U. Chai, Y. J. Choi, D. Kim, J. H. Park, *J. Phys. Chem. Lett.* **2017**, *8*, 2936–2940.
- [161] L. Zhang, B. Li, J. Yuan, M. Wang, T. Shen, F. Huang, W. Wen, G. Cao, J. Tian, *J. Phys. Chem. Lett.* **2018**, *9*, 3646–3653.

- [162] S. Zhang, S. Wu, W. Chen, H. Zhu, Z. Xiong, Z. Yang, C. Chen, R. Chen, L. Han, W. Chen, *Mater. Today Energy* **2018**, *8*, 125–133.
- [163] C. Dong, X. Han, Y. Zhao, J. Li, L. Chang, W. Zhao, *Sol. RRL* **2018**, *2*, 1800139.
- [164] W. Chen, H. Chen, G. Xu, R. Xue, S. Wang, Y. Li, Y. Li, *Joule* **2019**, *3*, 191–204.
- [165] Y. Guo, F. Zhao, J. Tao, J. Jiang, J. Zhang, J. Yang, Z. Hu, J. Chu, *ChemSusChem* **2018**, <https://doi.org/10.1002/cssc.201802690>.
- [166] C. F. J. Lau, M. Zhang, X. Deng, J. Zheng, J. Bing, Q. Ma, J. Kim, L. Hu, M. A. Green, S. Huang, A. Ho-Baillie, *ACS Energy Lett.* **2017**, *2*, 2319–2325.
- [167] F. Yang, D. Hirotani, G. Kapil, M. A. Kamarudin, C. H. Ng, Y. Zhang, Q. Shen, S. Hayase, *Angew. Chem. Int. Ed.* **2018**, *57*, 12745–12749; *Angew. Chem.* **2018**, *130*, 12927–12931.
- [168] D. Bai, J. Zhang, Z. Jin, H. Bian, K. Wang, H. Wang, L. Liang, Q. Wang, S. F. Liu, *ACS Energy Lett.* **2018**, *3*, 970–978.
- [169] W. Xiang, Z. Wang, D. J. Kubicki, W. Tress, J. Luo, D. Prochowicz, S. Akin, L. Emsley, J. Zhou, G. Dietler, M. Grätzel, A. Hagfeldt, *Joule* **2019**, *3*, 205–214.
- [170] L. Fu, Y. Zhang, B. Li, S. Zhou, L. Zhang, L.-W. Yin, *J. Mater. Chem. A* **2018**, *6*, 13263–13270.
- [171] D. Liu, C. Yang, M. Bates, R. R. Lunt, *iScience* **2018**, *6*, 272–279.
- [172] Y. Wang, T. Zhang, F. Xu, Y. Li, Y. Zhao, *Sol. RRL* **2018**, *2*, 1700180.
- [173] H. Rao, S. Ye, F. Gu, Z. Zhao, Z. Liu, Z. Bian, C. Huang, *Adv. Energy Mater.* **2018**, *8*, 1800758.
- [174] G. Yin, H. Zhao, H. Jiang, S. Yuan, T. Niu, K. Zhao, Z. Liu, S. Liu, *Adv. Funct. Mater.* **2018**, *28*, 1803269.
- [175] H. Jiang, J. Feng, H. Zhao, G. Li, G. Yin, Y. Han, F. Yan, Z. Liu, S. F. Liu, *Adv. Sci.* **2018**, *5*, 1801117.
- [176] H. Zai, D. Zhang, L. Liang, C. Zhu, S. Ma, Y. Zhao, Z. Zhao, C. Chen, H. Zhou, Y. Li, Q. Chen, *J. Mater. Chem. A* **2018**, *6*, 23602–23609.
- [177] Z. Guo, S. h. H. Teo, Z. Xu, C. Zhang, Y. Kamata, S. Hayase, T. Ma, *J. Mater. Chem. A* **2019**, *7*, 1227–1232.
- [178] Y. Zhou, X. Zhang, X. Lu, X. Gao, J. Gao, L. Shui, S. Wu, J.-M. Liu, *Sol. RRL* **2019**, DOI: 10.1002/solr.201800315.
- [179] S. Rühle, *Sol. Energy* **2016**, *130*, 139–147.
- [180] S. D. Stranks, *ACS Energy Lett.* **2017**, *2*, 1515–1525.
- [181] D. W. Niles, G. Margaritondo, *Phys. Rev. B* **1986**, *34*, 2923–2925.
- [182] J. Feng, Z. Yang, D. Yang, X. Ren, X. Zhu, Z. Jin, W. Zi, Q. Wei, S. Liu, *Nano Energy* **2017**, *36*, 1–8.
- [183] S. S. Bhosale, E. Jokar, A. Fathi, C.-M. Tsai, C.-Y. Wang, E. W.-G. Diau, *Adv. Funct. Mater.* **2018**, *28*, 1803200.
- [184] L. Yan, Q. Xue, M. Liu, Z. Zhu, J. Tian, Z. Li, Z. Chen, Z. Chen, H. Yan, H. L. Yip, Y. Cao, *Adv. Mater.* **2018**, *30*, 1802509.
- [185] Q. Zeng, X. Zhang, X. Feng, S. Lu, Z. Chen, X. Yong, S. A. T. Redfern, H. Wei, H. Wang, H. Shen, W. Zhang, W. Zheng, H. Zhang, J. S. Tse, B. Yang, *Adv. Mater.* **2018**, *30*, 1705393.
- [186] J. Zhang, D. Bai, Z. Jin, H. Bian, K. Wang, J. Sun, Q. Wang, S. F. Liu, *Adv. Energy Mater.* **2018**, *8*, 1703246.
- [187] Z. Jin, M. Yuan, H. Li, H. Yang, Q. Zhou, H. Liu, X. Lan, M. Liu, J. Wang, E. H. Sargent, Y. Li, *Adv. Funct. Mater.* **2016**, *26*, 5284–5289.
- [188] J. Zhang, Z. Jin, L. Liang, H. Wang, D. Bai, H. Bian, K. Wang, Q. Wang, N. Yuan, J. Ding, S. Liu, *Adv. Sci.* **2018**, *5*, 1801123.
- [189] Q. Chen, H. Zhou, T.-B. Song, S. Luo, Z. Hong, H.-S. Duan, L. Dou, Y. Liu, Y. Yang, *Nano Lett.* **2014**, *14*, 4158–4163.
- [190] J. Yuan, L. Zhang, C. Bi, M. Wang, J. Tian, *Sol. RRL* **2018**, *2*, 1800188.
- [191] Z. Zeng, J. Zhang, X. Gan, H. Sun, M. Shang, D. Hou, C. Lu, R. Chen, Y. Zhu, L. Han, *Adv. Energy Mater.* **2018**, *8*, 1801050.
- [192] H. Bian, D. Bai, Z. Jin, K. Wang, L. Liang, H. Wang, J. Zhang, Q. Wang, S. Liu, *Joule* **2018**, *2*, 1500–1510.
- [193] Y. Liu, Z. Hong, Q. Chen, W. Chang, H. Zhou, T. B. Song, E. Young, Y. M. Yang, J. You, G. Li, Y. Yang, *Nano Lett.* **2015**, *15*, 662–668.
- [194] H. Wang, H. Bian, Z. Jin, L. Liang, D. Bai, Q. Wang, S. Liu, *Sol. RRL* **2018**, *2*, 1800216.
- [195] M. Chen, M.-G. Ju, H. F. Garces, A. D. Carl, L. K. Ono, Z. Hawash, Y. Zhang, T. Shen, Y. Qi, R. L. Grimm, D. Pacifici, X. C. Zeng, Y. Zhou, N. P. Padture, *Nat. Commun.* **2019**, *10*, 16.

Manuscript received: January 26, 2019

Accepted manuscript online: March 12, 2019

Version of record online: August 27, 2019